

**ADAPTABLE WIND-POWERED FILTRATION SYSTEM
FOR RURAL WATER TREATMENT**

By John Campbell

A Thesis

**Submitted in Partial Fulfillment
of the Requirements for the Degree of
Master of Science
in Engineering**

Northern Arizona University

December 2010

Approved:

Thomas Acker, Ph.D. Chair

John Tester, Ph.D.

Paul Trotta, Ph.D.

ABSTRACT

ADAPTABLE WIND-POWERED FILTRATION SYSTEM FOR RURAL WATER TREATMENT

JOHN CAMPBELL

Sustainable, low-cost water treatment systems are critical elements to developing nations and remote off-grid areas of the developing world. According to the World Health Organization, water and sanitation are the primary drivers of public health. This research will build on proven theory and technology to develop an adaptable, affordable and sustainable system for treating drinking water in off-grid rural environments. Components of this design will be analyzed and tested for application in rural Africa through a Northern Arizona University (NAU) Engineers Without Borders (EWB) Student Chapter project in Ghana. An annual average wind speed of 3.5 m/s at a height of three meters is assumed with surface water fecal bacteria levels not exceeding 300/100 ml sample. The system is designed to use readily available, low-cost materials and renewable wind energy to treat contaminated surface waters in order to make clean drinking water more accessible to communities in need. The design chosen utilizes a Savonius rotor used in conjunction with a positive displacement pump to move water through a biological slow sand filter. Power curves for a specified Savonius rotor design are found experimentally and allow for estimation of the water treatment system output. Results indicate that this system will be able to provide clean drinking water for up to 575 people.

Table of Contents

ABSTRACT.....	2
Chapter 1: Introduction	8
1.1 The Problem.....	8
1.2 Specific Objectives	9
1.3 The Problem Statement	9
1.4 Report Layout.....	10
Chapter 2: System Design Requirements	11
2.1 Qualitative System Requirements	11
2.2 Quantitative System Requirements.....	12
2.2 Potential Design Solutions	13
Water Treatment System.....	13
Water Movement System.....	14
Chapter 3: Water Treatment System.....	15
3.1 Biological Slow Sand Filtration Background.....	15
3.2 System Components	16
3.3 Parallel Filter plumbing.....	17
3.4 Grain Size and Uniformity coefficient.....	18
3.5 Sand bed depth	19
3.6 Flow rates and removal rates	19
3.7 Storage tanks	20
3.8 Operations and Maintenance	20
Chapter 4: Pump selection.....	22
Chapter 5: Turbine Design Process	23
5.1 Savonius Rotor Design	23
5.2 Hardware Requirements.....	25
5.3 Power Transfer Design.....	26
5.4 Structural Design.....	28
Frame Analysis	28
Shaft Analysis	30
Guy Wire Analysis	31

Chapter 6: Experimental Analysis	33
6.1 Testing Plan	33
6.2 Experimental Setup	33
Data Acquisition Hardware and Software	33
Torque Measurement	35
Shaft Speed Measurement	37
Wind Speed Measurement	38
6.3 Processing Data	39
Power Curves	39
Pump Curves	40
6.4 Experimental Results	40
Turbine	40
Uncertainty Analysis	44
Turbine and pump combined	45
Instantaneous Flow rate	45
Average Flow rate	46
Chapter 7: Journal Article Submission	49
7.1 Journal Manuscript	49
Chapter 8: Conclusions	50
8.1 Combined system overview	50
8.2 Design Requirements Results	50
Qualitative Requirements	50
Quantitative Requirements	51
Works Cited	52
Appendices	54

List of Tables

Table 1: Water treatment system options and decision matrix.	13
Table 2: Water movement system options and decision matrix.	14
Table 3: Experimentally derived removal rates (Muhammad, 1996).....	19
Table 4: Typical parameters for positive displacement pumps (Fraenkel, 1986).....	22
Table 5: Frame analysis	29
Table 6: Hollow Shaft Fatigue Analysis.....	31
Table 7: Theoretical power output.....	43
Table 8: Daily average flow rates (lit/day) VS annual average wind speed.....	48

List of Figures

Figure 1: Shallow well located in northern Ghana	8
Figure 2: Household biological slow sand filter (CAWST, 2009)	16
Figure 3: Water treatment system one-line diagram.....	17
Figure 4: Plumbing for parallel biological slow sand filters (Borger, et al., 2005).....	18
Figure 5: Typical results from a sieve analysis.....	18
Figure 6: Windmill Tower (Brace Research Institute, 1973)	23
Figure 7: Savonius rotor variables (Menet, 2002)	24
Figure 8: Double step Savonius rotor	25
Figure 9: Pillow Block bearing	25
Figure 10: Flange Mounted bearing.....	25
Figure 11: Rod-end	26
Figure 12: Power transfer mechanism	26
Figure 13: Bell crank distance traveled ratio	27
Figure 14: Frame vertical support loading.....	29
Figure 15: Turbine shaft loading regime	30
Figure 16: Guy wire loading regime.....	31
Figure 17: Data Acquisition One-line Diagram.....	33
Figure 18: NI SC-2350 Signal Conditioning	34
Figure 19: NI 6024E Data Acquisition Card	34
Figure 20: LabVIEW Front Panel.....	35
Figure 21: LabVIEW Block Diagram.....	35
Figure 22: Turbine experimental setup	36
Figure 23: NI SCC-SG Series Strain Gauge Input Module	36
Figure 24: Torque sensor calibration experimental setup.....	37
Figure 25: Shaft speed sensor	38
Figure 26: NI SCC-FT01 feed through module.....	38
Figure 27: NRG #40C calibrated anemometer	38
Figure 28: Computational flow analysis around a mast (Filippelli, et al., 2005)	39
Figure 29: Power curve for 1-3 N*m loading	40
Figure 30: Power curve for 3-5 N*m loading.....	40
Figure 31: Power curve for 5-7 N*m loading.....	41
Figure 32: Power curve for 7-9 N*m loading.....	41
Figure 33: Summary of turbine power curves for various loadings	41
Figure 34: Performance of conventional wind turbines (Menet, 2002).....	42
Figure 35: Collected data and predicted power	43
Figure 36: Uncertainty calculation points.....	44
Figure 37: Instantaneous flow curve for turbine loading 5-7 N*m	46
Figure 38: Rayleigh Probability Density Function at four average wind speeds	47
Figure 39: Annual average flow rates VS annual average wind speeds	47
Figure 40: Complete water treatment system including storage.....	50

Nomenclature

A_p	area of the piston (m^2)
A_t	area of the turbine (m^2)
c	distance from shaft center line where the stress is calculated (m)
C_d	coefficient of drag
d	diameter of each rotor scoop
D	diameter of rotor
d_{10}	Effective grain size
D_f	diameter of end plates
e	gap between main paddles: main overlap
F	force (N)
F_d	force of drag (N)
F_t	force of tension (N)
F_x	force in the x axis (N)
F_y	force in the y axis (N)
g	acceleration of gravity (m/s^2)
h	height of water (m)
H	height (m)
H_p	pump head (m)
I	moment of inertia (kg/m^2)
k_a	surface condition modification factor
k_b	size modification factor
k_c	load modification factor
k_d	temperature modification factor
k_e	reliability factor
k_f	miscellaneous factor
L	length (m)
M	moment ($N*m$)
M_{max}	maximum moment ($N*m$)
N	Newton
NTU	Nephelometric Turbidity Units
P	power (Watts)
P_{fluid}	pressure of the fluid (Pascal)
Q	volumetric flow rate (m^3/s)
q	distributed load (N/m)
S_e	endurance limit (Pascal)
S'_e	test specimen endurance limit (Pascal)
S_{ut}	ultimate stress (Pascal)
S_y	yield stress (Pascal)
T	torque ($N*m$)
U	sand grain uniformity coefficient
V	wind Velocity (m/s)
\bar{V}	average wind velocity (m/s)
W	work (joules)
y	distance from beam center line where the stress is calculated (m)
β	overlap ratio
Δd	displacement (m)
Δx	displacement along the x axis (m)
Δy	displacement along the y axis (m)
η	pumping efficiency (%)
ρ	fluid density (kg/m^3)
σ	stress (Pascal)
σ_{inf}	bending stress for infinite life (Pascal)
ω	angular velocity (rad/s)

Chapter 1: Introduction

1.1 The Problem

“Close to a billion people are still without access to improved water supplies, half of whom live in the African and Western Pacific Regions” (World Health Organization, 2009). This results in 41% of the people in Africa having no access to clean water. This same report indicates that the majority of the 41% are from lower income families located in rural areas. This creates engineering design constraints that are quite challenging. Most often, an unimproved water source is available, but this water usually contains harmful contaminants. An example of an unimproved water source can be seen in Figure 1.



Figure 1: Shallow well located in northern Ghana

Water sources like this example are scattered across northern Ghana, and are prevalent throughout underdeveloped areas of the world. Working in northern Ghana with the Northern Arizona University Engineers Without Borders Chapter, it was discovered that a large majority of people use water from sources such as these for drinking. Upon further investigation, the quality of this water is extremely poor (see Appendix 1). The effects of consuming water of this quality causes a myriad of health issues. “Poor water quality can increase the risk of such diarrheal diseases as cholera, typhoid fever and dysentery, and other water-borne infections.” (World Health Organization, 2010)

1.2 Specific Objectives

This report is a technical design report. The specific objectives of this report are as follows:

1. Form the problem statement.
2. Define the qualitative requirements that must be met
3. Define the quantitative requirements that a solution must meet
4. Identify alternative methods for solving stated problem
5. Select the most advantageous solution to the problem
6. Provide detailed design specification for proposed solution
7. Perform experimental analysis on aspects of the design that must be tested.
8. Summarize the findings and draw conclusions as to how well the solution meets specific design criterion.
9. Submit findings for publication.

1.3 The Problem Statement

Addressing the problem of purifying contaminated water requires a water purification system that is simple, reliable, affordable, sustainable, and effective.

1.4 Report Layout

The specific objective for this design solution report will be addressed in the following order:

Chapter 1: Introduction

This chapter will address objective 1, giving a background into the lack of available clean drinking water around the world.

Chapter 2: System design

This chapter will address objective 2-5, first laying out the design requirements, then discussing design alternatives by weighing options using a basic decision matrix. From these design requirements and decision matrices, a specific solution to the problem statement will be selected.

Chapter 3: Water filtration

This chapter will address objective 6, specifically related to the design specifications for the water filtration portion of the solution.

Chapter 4: Pump Selection

This chapter will address objective 6, specifically related to the selection of a pump.

Chapter 5: Wind Turbine

This chapter will address objective 6, specifically related to the design specifications for the wind turbine portion of the solution.

Chapter 6: Design testing

This chapter will address objective 7, addressing the testing plan, detailing the experimental setup, and discussing experimental results.

Chapter 7: Journal Article Submission

This chapter will address objective 9. This chapter is a copy of the document that will be submitted for publication that summarizes the findings of this thesis.

Chapter 8: Conclusion

This chapter will address objective 8, drawing conclusions on how well the solution meets the design requirements.

Chapter 2: System Design Requirements

2.1 Qualitative System Requirements

The qualitative system requirements are a set of parameters in which the system must function to be a viable solution to the problem statement. The concept for this system came while working in a rural area of Northern Ghana. While a majority of the qualitative system requirements came with the idea of installing the system in this area, the system solution could be applied to other areas with similar qualitative system requirements.

Simple

Appropriate technology must be selected. An overly complex system would be problematic, as operations and maintenance of such a system would be difficult in a rural environment. The system should be easily understood and operated by someone with very little formal education.

Reliable

Drinking water is such an important driver in human health. The solution must be able to provide water to its users consistently with minimal down time. Replacement parts should be readily available should something break.

Affordable

The lack of available clean water can be closely correlated to people in impoverished areas of the world. The system should be affordable based on the average income of the area in which it will be installed. The cost of water should be less expensive than that of other local sources of safe drinking water.

Sustainable

The system should operate in a sustainable manner. This means being funded, owned and operated by the individuals using the water supply. The system must also operate independent of outside power source i.e. electrical grid.

Effective

The system must clean water effectively. This means meeting local drinking water standards. In the event that there are no local standards, the system must meet globally accepted water quality standards.

2.2 Quantitative System Requirements

The quantitative system requirements are a set of parameters in which the system must function to be a viable solution to the problem statement. The concept for this system came while working in a rural area of Northern Ghana. While a majority of the quantitative system requirements came with the idea of installing the system in this area, the system solution could be applied to other areas with similar quantitative system requirements.

Contaminants

This system targets water supplies that contain moderate levels of microbial contaminants, specifically faecal coliform. The solution need not target the removal of chemical contaminants, nor does it need to treat heavily contaminated water (i.e. black water). Faecal coliform levels of raw water should not exceed 300/100 ml sample. The target is complete removal, but up to 10/100 ml sample is allowable.(United Nations Environment Programme Global Environment Monitoring System, 2007)

Flow Rates

There are a number of solutions to this problem statement that provide water for a single family. This system should focus on providing flow rates that meet the water requirements for multiple families (about 25 people) to a small community (500 people). The World Health Organization estimates that the required daily water usage for drinking and cooking per person is 7.5 liters or about 2 gallons.(World Health Organization, 2003)

Pump Head

Contaminated water can come from a variety of sources. For this research, water that is easily accessible for everyday drinking will be considered, and thus the maximum pump head that this system should be required to handle is 30 meters. Contaminated water sources could consist of a stream, lake, pond, rain catchment, or an open air well.

Weather

The system must operate in weather similar to Ghana. This assumes a solar resource of 5.5 kWh/m² per day (Bailey, 2007) and a wind power class 2, marginal resource potential 6.2-7.1 m/s at 50 meters.(U.S. Department of Energy, 2004) This value relates to about 3.4 m/s at 5 meters.

Robust

Components selected to be used in the system must be robust. This requires that components be designed to last a minimum of one year. Corrosion, fatigue, strength, brittleness, and similar design criterion should be considered.

2.2 Potential Design Solutions

Now that both the qualitative and quantitative system requirements have been established, potential design solutions can be explored. To do this effectively, this system will be broken into two smaller systems: water movement and water treatment. The water movement system will deal with transporting the surface water; while the water treatment system will cover all aspects of contaminate removal.

Water Treatment System

There are many different types of water treatment systems that could meet the needs of the problem statement. Table 1 shows a decision matrix with the design alternatives being considered.

Table 1: Water treatment system options and decision matrix.

	Simple	Reliable	Affordable	Sustainable	Effective	Flow Rates	Robust	Total
Slow Sand filtration	10	8	8	9	3	5	5	48
Biological Slow sand filtration	8	8	8	9	8	5	5	51
Rapid Sand filtration with Chlorine disinfection	1	4	4	2	9	5	5	30
Membrane Filtration (microfiltration)	4	6	2	4	9	5	5	35
Membrane Filtration (nanofiltration)	4	5	0	4	10	5	5	33
Manual Chlorination	2	4	7	2	9	4	5	33

Simplicity is one of the driving factors for this decision matrix. This causes any solution with chlorine to drop out, as chemical dilutions can be quite complicated. These chlorine solutions also scored low in sustainability as the cost and availability of chlorine could be an issue. Cost was by far the major driver in this decision matrix. Membrane filtration requires the use of costly filters that must be replaced. Although this form of treatment is extremely effective, the solution is cost prohibitive. Lastly, the decision between biological slow sand filtration, and basic slow sand filtration was driven by

effectiveness. Slow sand filtration with no biological treatment would result in ineffective water treatment, and thus biological slow sand filtration was chosen as the solution for water treatment.

Water Movement System

There are many different types of water movement systems that could meet the needs of the problem statement. Because one of the requirements is that the solution must be self contained, the solution must provide its own power to move the water. Table 2 shows a decision matrix with the design alternatives being considered.

Table 2: Water movement system options and decision matrix.

	Simple	Reliable	Affordable	Sustainable	Flow Rates	Pump Head	Weather	Robust	Total
Solar powered DC pump	5	3	2	5	5	5	9	3	37
Typical three blade turbine with electrical pump	4	3	4	5	5	5	3	5	34
Typical three blade turbine with mechanical pump	6	5	6	8	5	5	3	5	43
American windmill with mechanical pump	7	7	7	7	5	5	7	5	50
Savonius Windmill with mechanical pump	9	7	9	8	5	5	7	5	55
Manual hand pump	10	8	10	4	1	5	5	5	48

Appropriate technology is one of the driving factors for this decision matrix. Because of the location, parts for more advanced technologies are often difficult to obtain, and technicians that can service these technologies are not available. This pushes the decision matrix to favor mechanical systems rather than electrical systems, thus the low scores for the first two solutions. The next big driving factor is the weather. A typical three-blade wind turbine utilizes an airfoil that produces lift, while the American windmill and the Savonius windmill primarily utilize drag force. The drag machines produce higher torque and operate at much lower wind speeds than lift machines. This high torque is advantageous when pumping water. The manual pump also scored well, but had a hard time meeting the flow rates required. This is due to the time demand required. Pumping water would have to be someone's full-time job, which is not practical. Lastly, the ease of manufacturing and low construction cost give the Savonius windmill a slight advantage over the American windmill, and thus the Savonius windmill with a manual pump was selected for the water movement system.

Chapter 3: Water Treatment System

3.1 Biological Slow Sand Filtration Background

Biological slow sand filtration (BSSF) has been used in rural settings and has proven itself as an appropriate technology for conditions found in Africa. "No other single process can effect such an improvement in the physical, chemical and bacteriological quality of surface waters" (Huisman, et al., 1974). BSSF utilizes both physical and biological treatment of water. Physical treatment is an effect of mechanical filtration, and the biological treatment is a result of the development of a biological layer on the top later of sand (Muhammad, 1996). This biological layer will be referred to as a biofilm.

The discovery of the effectiveness of BSSF in intermittently operated filtration has led to its widespread use. This allows the filter to be loaded with contaminated water on an as needed basis. In the past, most slow sand filters required continuous operation, because it was believed that the biofilm must be constantly supplied with both oxygen and a food source. Perceptions changed as lab results showed that the biofilm could be supplied with oxygen through diffusion if the water level is held just above the biofilm. This has led to the use of small household water treatment filters. There are quite a few different designs, but all of these filters operate on the same principle. An example of such a filter can be seen in Figure 2. Notice that the light green layer below the diffuser represents the biofilm.

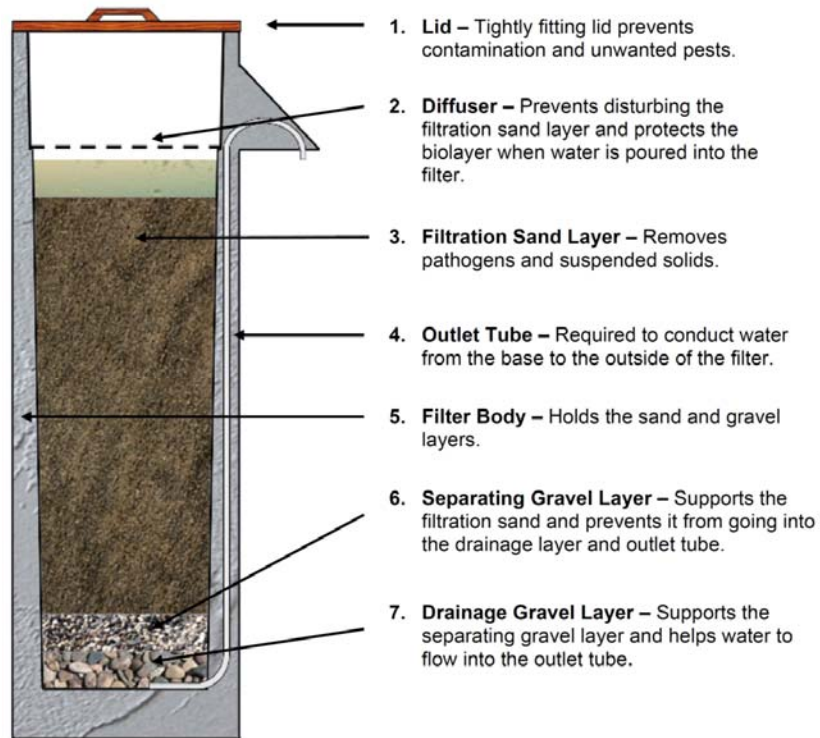


Figure 2: Household biological slow sand filter (CAWST, 2009)

With the effluent pipe above the top of the fine sand, the water level should never drop below the biofilm. The removal rates for these types of filters are impressive despite their simplicity. These household filters can be scaled up to provide water for larger families or communities.

3.2 System Components

The design for the filter system is comprised of three components, pre-filter storage, biological slow sand filters, and post-filter storage. In the event of the surface water being highly turbid (greater than 50 NTU), a roughing filter can be added as a fourth component. This prevents premature clogging of the filters. A one-line diagram showing how water flows through these components can be seen in Figure 3.

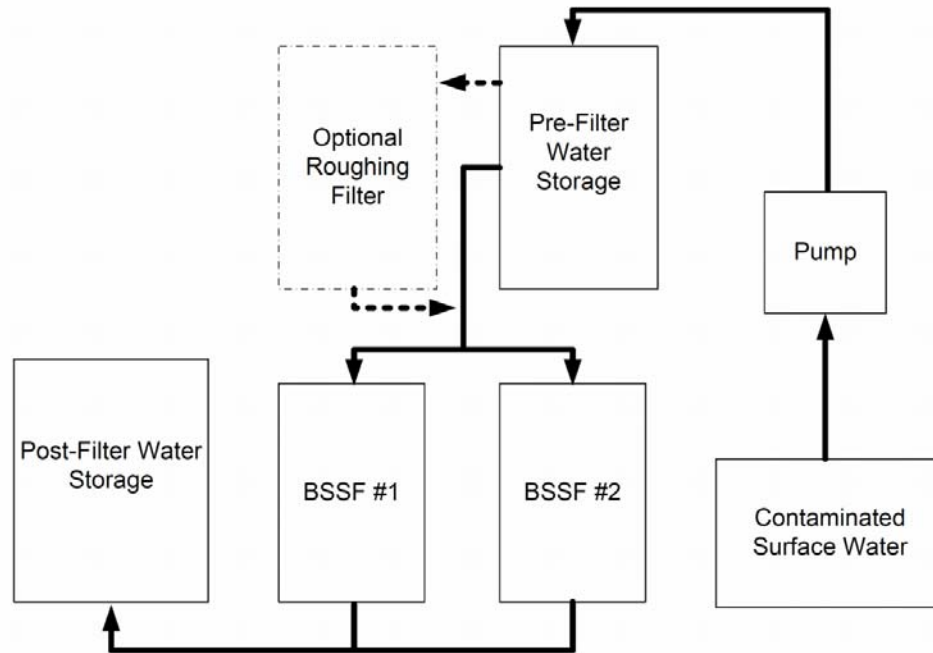


Figure 3: Water treatment system one-line diagram.

To increase the cost effectiveness of the solution, each of the system components will utilize 55 gallon drums. Polypropylene drums are preferred over steel drums, as they are more resistant to corrosion. This design selection allows the system to be modular. If the post-filter storage size must be increased, another drum can be added. In this way, a system can be sized to meet specific application requirements.

3.3 Parallel Filter plumbing

Because filter cleaning requires downtime, during which it is desirable to have continued access to clean water, the design places two filters in parallel. This allows one filter to be cleaned, while the other can remain in operation. A diagram of the plumbing layout for the parallel biological slow sand filters can be seen in Figure 4 and can be seen in greater detail in Appendix 2.

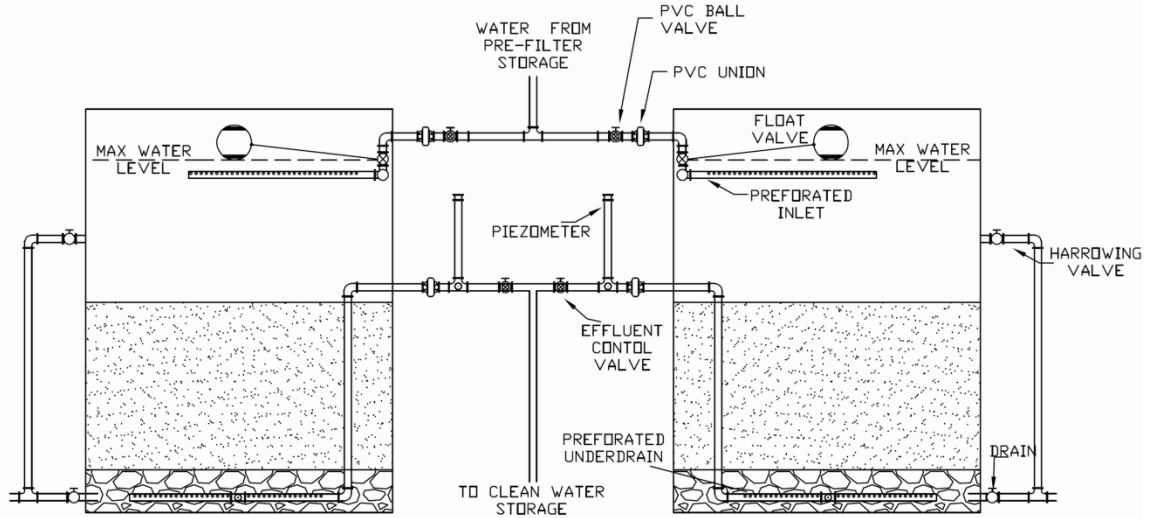


Figure 4: Plumbing for parallel biological slow sand filters (Borger, et al., 2005).

3.4 Grain Size and Uniformity coefficient

The effective grain size and uniformity coefficient play important roles in the removal rates for a BSSF. The effective size of sand, d_{10} , is defined as the value at which 10% of the grains are smaller, and 90% of the grains are larger. This can be found using a sieve analysis.

The uniformity coefficient is defined by

$$U = \frac{d_{60}}{d_{10}} \quad (1)$$

Here d_{60} is found in a like manner as d_{10} but 60% of the grains are smaller, and 40% of the grains are larger. Figure 5 shows how where these values can be found when graphing the results of a sieve analysis.

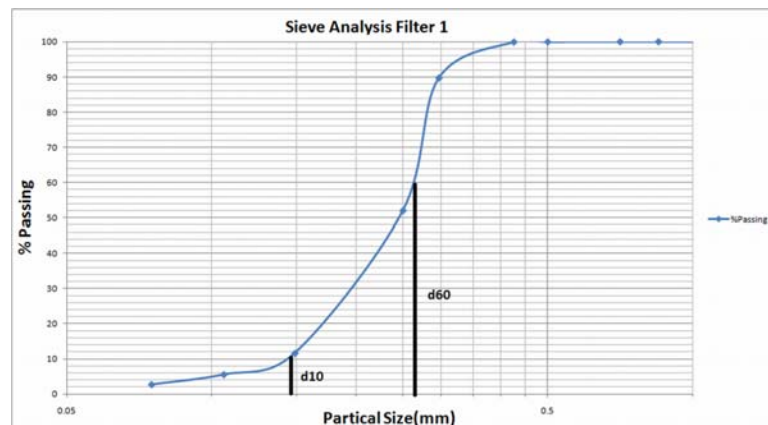


Figure 5: Typical results from a sieve analysis.

Because these factors affect removal, an effective grain size of .35mm with a uniformity coefficient of 2 has been chosen to standardize this design. These parameters were chosen to extend filter runtime between cleanings, while maintaining adequate removal rates (Muhammad, 1996).

3.5 Sand bed depth

The depth of the sand does affect the removal rates, but not very drastically. Research has shown that a sand bed depth of 45 cm is sufficient for the target removal rates of 99% (Muhammad, 1996). The filter is constructed from a drum. The drum should be filled to 50 cm. During cleaning, some sand may be removed. When the sand level reaches 45 cm, more sand should be added to the 50 cm mark.

3.6 Flow rates and removal rates

Flow rates for BSSF can have a dramatic affect on the removal rates. Low flow rates increase removal rates, but if flow rates become too high, the likelihood of decreased removal rates and parasitic breakthroughs increases. For this reason, the filter has been designed to operate at or below 1 m/hr once the biofilm layer has fully developed. The volumetric flow rate can be found using this linear flow rate by multiplying by the cross sectional area of the filter. The cross sectional area of a standard 55 gallon drum will require an average flow rate of about 5 liters per minute to keep the filter constantly loaded. With the grain size, uniformity coefficient, and flow rate determined, Table 3 shows the estimated removal rates for faecal coliform, total coliform, turbidity and color.

Table 3: Experimentally derived removal rates (Muhammad, 1996)

Filtration Rate (m/hr)	Average % Removal			
	FC	TC	Turbidity	Colour
0.1	99.60	99.70	96.50	95.10
0.2	98.70	98.90	90.10	93.80
0.3	98.30	98.10	89.10	89.60

With these removal rates, this treatment system can treat raw water with a faecal coliform concentration of 1400/100ml sample, and still stay below the maximum allowable concentration of 10/100ml sample (United Nations Environment Programme Global Environment Monitoring System, 2007).

As the filter becomes clogged, the flow rates will decrease. When the flow rate drops below an acceptable level, the filter must be cleaned.

3.7 Storage tanks

Because the flow rates for BSSF are relatively slow, pre-filter storage and post-filter storage allows the system to treat water continuously and meet demand for a reliable clean water supply. Proper sizing of these storage tanks will ensure successful system operation.

Pre-filter storage allows water that is pumped during higher wind speeds to be stored, and processed by the filters when wind speeds are lower. The lower the average wind speed, the larger your pre-storage requirement. Assuming a distribution of wind speeds described by the Rayleigh distribution (explained in detail in the results section) one can predict the amount of time that the pump will be providing water at a flow rate larger than the filter can process. The pre-filter storage should be sized using the percentage that the pump will be providing less than the filter can process. This value applied by the hourly flow rate will give an estimate of the cushion provided by the pre-filter storage.

Post-filter storage allows water that is processed to be stored before being used. This is especially important, as water processed at night can be used during the day. To store all the water that has been pumped during the night, half of the daily flow will be required for storage. This may result in a very large post-filter storage, and decisions on storage size need to be balanced with cost.

3.8 Operations and Maintenance

Although BSSF is a simple process, there are certain precautions that must be taken to ensure that the system effluent is maintained at a satisfactory level. The first step in ensuring that this takes place is allowing adequate time for the biofilm to develop. This is done by letting the filter operate at the design flow rate. The rate at which the biofilm will develop varies as a function of influent water quality and temperature. During this time, water from the filter should not be used. When the biological layer has developed, testing of the raw water and from the effluent should be taken to verify that the filter is performing at the desired removal rates. This process can take two weeks to a month.

Once the biofilm has developed, the filter can be operated at the design flow rate. The flow rate should be monitored, and adjusted using the effluent control valve shown in Figure 4. When the flow rate drops below .5 m/hr the filter has become clogged, and will need to be cleaned. The mean time to maintenance varies widely based on local conditions. The factors that are most influential are water turbidity, flow rates, temperatures, and the specific contaminants within the water. The maintenance schedule needs to be determined in the field.

With two filters operating in parallel as shown in Figure 4, one filter should be cleaned while the other remains in service. The cleaning process that will allow the filter to be down the least amount of time is a process called “wet harrowing”. This requires the effluent control valve to be closed. The filter is then filled with water and the surface is agitated by swirling the water manually. Water is then removed by opening the harrowing valve. This process is repeated until a significant amount of biomass has been removed from the filter. This process is one of the easiest maintenance procedures for slow sand filters and allows the biofilm to redevelop in about seven days. Before the filter is placed back into service, testing from the raw water and from the effluent should be taken to verify that the filter is performing at the desired removal rates.

Chapter 4: Pump selection

This system is designed to use a positive displacement pump. With this in mind, a pump that has locally available replacement parts, or can be constructed with locally available material should be selected. Table 4 shows some pump selection parameters.

Table 4: Typical parameters for positive displacement pumps (Fraenkel, 1986)

Pump Type	Head Range (m)	Input Power (kW)	Flow Range (m ³ /h)	Efficiency (%)
Piston/Bucket pumps	5-200+	.03-50+	2-100+	40-85
Plunger pumps	40-400	.50-50+	2-50+	60-85
Diaphragm pumps	1-2	.03-5	2-20	20-30

With these values in mind, pump diameter, pump stroke, pump head, and cost should all be taken into consideration when selecting a pump. An example of sizing a pump to a specific turbine loading target can be found in Section 5.3 and may assist in pump selection.

Chapter 5: Turbine Design Process

Moving water through biological slow sand filters requires energy. In a rural setting, where electricity isn't available, options for moving water are limited. Because the flow rates required for BSSF are relatively low, it becomes challenging to consistently keep the filter manually loaded. It can become a full time job to constantly add water to the filter. The design solution proposed here utilizes a wind powered pump to keep water constantly moving through the filter and producing clean water. For the windmill, a Savonius turbine has been selected, as displayed in Figure 6.

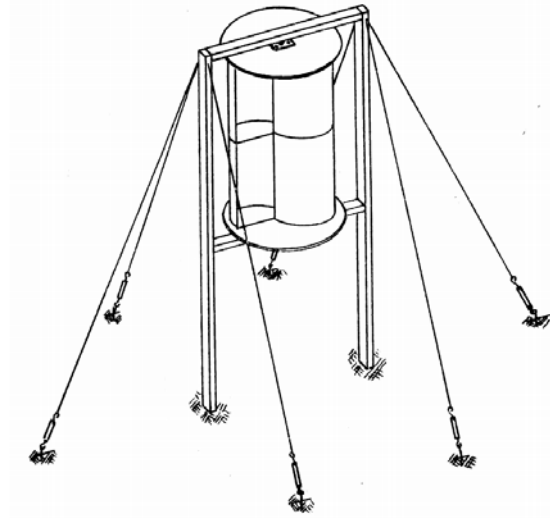


Figure 6: Windmill Tower (Brace Research Institute, 1973)

A Savonius wind turbine was selected for this application due to its low start-up speed, high torque characteristics, and its ability to function in areas with low to moderate wind resources. In this design, the rotor is built from two 55 gallon oil drums (or similar drums available locally). The structure (tower) upon which the rotor will be mounted elevates the base of the rotor approximately 3 meters above the ground, as depicted in Figure 6. The tower is designed to be built out of wood, creating a fairly ridged structure, with concrete footers at the base. Guy wires made of 1/8 inch galvanized steel cable support the structure

5.1 Savonius Rotor Design

The rotor is designed to be built out of two steel or polypropylene barrels that are cut in half and then mounted on plywood endplates. When designing a Savonius rotor,

there are several geometric variables that can be changed. These variables can drastically change the performance of the rotor. Figure 7 shows these variables.

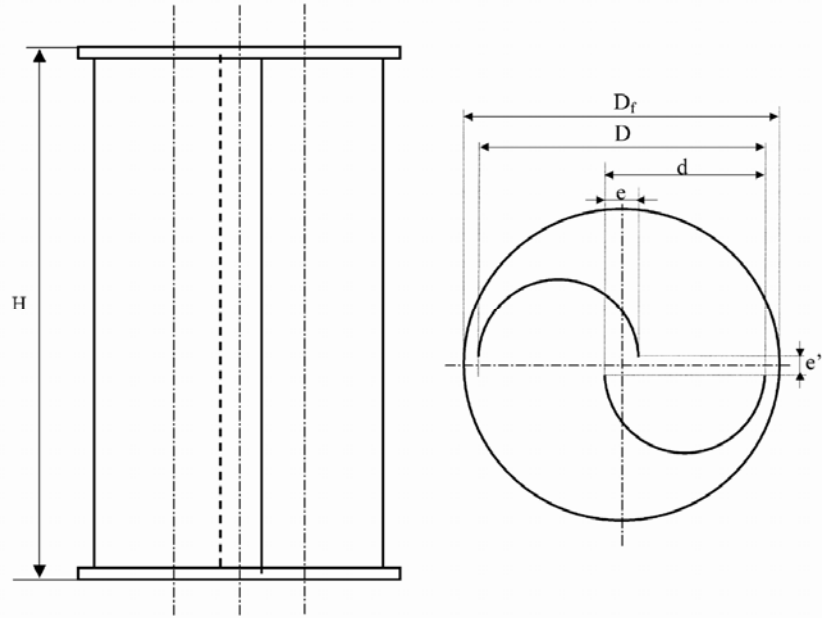


Figure 7: Savonius rotor variables (Menet, 2002)

The overlap ratio is one of the most influential design parameters of the Savonius rotor and is defined as

$$\beta = \frac{e}{d} \quad (2)$$

The variables e and d can be found in Figure 7. After extensive wind tunnel testing, it has been determined that the most efficient overlap is between 20% and 30% (Menet, 2002). With this in mind, the design selected calls for an overlap ratio of 25%. With a rotor made from a standard steel, or polypropylene barrel, this overlap is 22 cm. End plates have also proven to increase the efficiency of a Savonius rotor. It has been shown that a value of D_f 10% greater than D provides the most efficient increase in performance with the least amount of material (Ushiyama, et al., 1988). Lastly, the rotor has been designed to be a “double step” rotor. This means that the top half and the bottom half will be offset by 90° . This will provide a more efficient rotor as well as higher and more consistent start up torques (Ushiyama, et al., 1988). This will require a plate in between the upper half and the lower half of the rotor. Figure 8 depicts an example of what this rotor might look like.



Figure 8: Double step Savonius rotor

5.2 Hardware Requirements

One of the most important hardware requirements for this design is the bearings that allow the turbine shaft to rotate. These bearings are crucial to the success of the wind turbine. Bearings for the turbine must be rated to carry a 3500 N thrust load. The bearings must also be rated as self-aligning. As the turbine experiences high winds, the frame will shift. Self-aligning bearings have the ability to rotate within a socket, and prevent the bearings from experiencing unnecessary loading. These bearings can be found as pillow block bearing and as flange mount bearing, as can be seen Figure 9 and Figure 10. Both mounting styles can be used.



Figure 9: Pillow Block bearing (DIY Trade)



Figure 10: Flange Mounted bearing (Global Spec)

Another crucial hardware requirement is the use of rod-ends for all of the power transfer junctions. The design calls for three. The first connects the eccentric to the connecting rod, the second connects the connecting rod to the bell crank, and the third connects the bell crank to the pump rod all shown in Figure 12. These rod-ends allow for critical rotation in the linkage, as well as reduce the power transfer losses. The rating required will be determined by the maximum force occurring in the power transfer mechanisms. An example of a rod-end can is displayed in Figure 11.



Figure 11: Rod-end (Kaeding Performance)

5.3 Power Transfer Design

The power transfer mechanism, which changes the rotational output of the Savonius rotor to the reciprocating motion used by the pump, is illustrated in Figure 12.

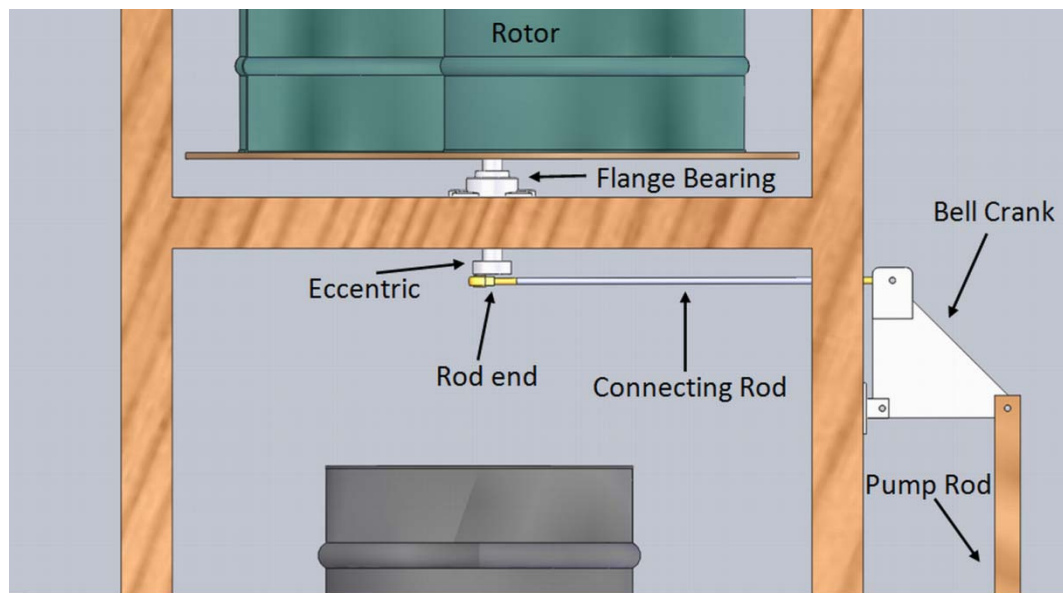


Figure 12: Power transfer mechanism

The power transfer system consists of the eccentric, the connecting rod, the bell crank, and the pump rod. These pieces work together to transfer power from the turbine shaft to the pump. The power transfer components are designed to match the desired turbine loading with a specific pump. To get an idea of size, dimensioned drawings can be seen in Appendix 3 and Appendix 4.

The radius of the eccentric should be kept small compared to the diameter of the turbine. The larger the radius of the eccentric, the larger the angle fluctuation between the connecting rod and the turbine frame. This can be minimized by restricting the eccentric radius to no larger than 1/10 the turbine radius. A ratio of 1/20 has been chosen simply because a small piece of bar stock can be welded along the side of the turbine shaft. The connecting rod should have a threaded section to allow for adjustment in length. The length of the connecting rod should be such that when the eccentric is at its furthest position from the bell crank, the vertical section of the bell crank is parallel to the frame. The bell crank dimensions can be adjusted to change the power transfer ratio from the connecting rod to the pump rod. The ratio of distance traveled per stroke is directly proportional to the dimensions of the bell crank as seen in Figure 13.

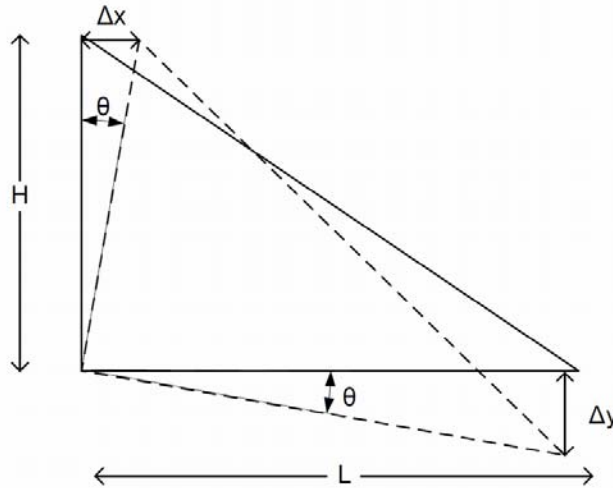


Figure 13: Bell crank distance traveled ratio

This can be seen with the following geometric proof.

$$\Delta y = \sin(\theta) L \quad \text{and} \quad \Delta x = \sin(\theta) H \quad \text{therefore}$$

$$\frac{\Delta x}{\Delta y} = \frac{\sin(\theta) H}{\sin(\theta) L} \quad \text{or} \quad \frac{\Delta x}{\Delta y} = \frac{H}{L} \quad (3)$$

Given that

$$W = F\Delta d \quad (4)$$

The conservation of work through the bell crank determines that

$$\frac{H}{L} = \frac{F_x}{F_y} \quad (5)$$

The bell crank allows the designer the ability to change both the pumping stroke, and the pumping force. Take for example, a piston pump with a diameter of 5 cm and 15 meters of pump head. The pressure that must be applied to the piston to overcome the water pressure is found by

$$P_{\text{fluid}} = \rho gh \quad (6)$$

With the given parameters, this results in a pressure of about 148 kPa. With the force on the piston found by

$$F = P_{\text{fluid}}A_p \quad (7)$$

For the given parameters, this results in a force on the piston of about 289 N. Let's assume that the required turbine loading is 6 N*m. With an eccentric diameter ratio of approximately 1/20, the radius of the eccentric is 2.38 cm or .0238 m. Dividing the turbine loading by the moment arm (radius) of the eccentric provides the target force on the connecting rod of about 252 N. With these values and Equation (5) we can determine the correct ratio for the bell crank. For this example a bell crank with an H/L ratio of .87 will provide the target loading of the turbine.

5.4 Structural Design

All portions of the structural analysis of this turbine will be based on a survival wind speed of 90mph. Based on this wind speed, each section of the turbine that will be under analysis will be expressed in factors of safety (FS).

Frame Analysis

The frame of this turbine will encounter loading at a variety of angles and intensities. The most vulnerable portion of the frame is the long, vertical uprights. These can be seen in Figure 6. The wooden timber that makes up the wind turbine frame can be simplified to a simply supported beam. This beam has a distributed load on half of the beam. An example of this loading can be seen in Figure 14.

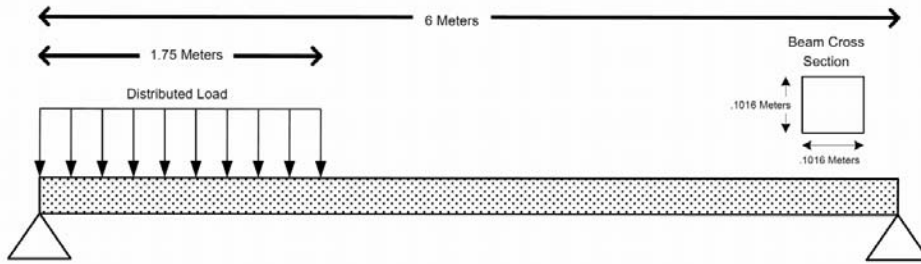


Figure 14: Frame vertical support loading

Because the shape of this turbine is unique, there are no predetermined drag coefficients available, and could only be determined experimentally. This experiment is outside the scope of this research. For this reason the system was simplified to a flat plate perpendicular to flow (White, 2003).

$$C_d = 1.28 \quad (8)$$

Using this value, the force of drag on the turbine can be found using by (Manwell, et al., 2002)

$$F_d = \frac{1}{2} \rho V^2 A_t C_d \quad (9)$$

The maximum bending stress in the upright member of the turbine can be found by (Beer, et al., 1992)

$$\sigma = \frac{My}{I} \quad (10)$$

An average ultimate stress for wood of 32,200 KPa is assumed (Green, et al., 1999) based on the average value for 113 types of commercial lumber. One standard deviation below the average is assumed. Table 5 shows the values calculated for this frame analysis.

Table 5: Frame analysis

Givens			Calculated Values		
Base	0.1016	m	F_d	1810.19	N
Height	0.1016	m	M	2715.29	$N \cdot m$
Density	1.01	$\frac{kg}{m^3}$	I	8.8796E-06	
V	90.00	mph	Calculate Stress	15,503,544	Pa
V	40.23	$\frac{m}{s}$	FS	2.08	
A	1.73				
C_d	1.28				
Y	0.0507	m			
Strength Ult.	32,200,000	Pa			

Shaft Analysis

The shaft for this turbine has been designed to withstand the fatigue loading that it will encounter as it rotates. This analysis is for a simply supported rotating hollow shaft, with a distributed load. The loading regime can be seen in Figure 15.

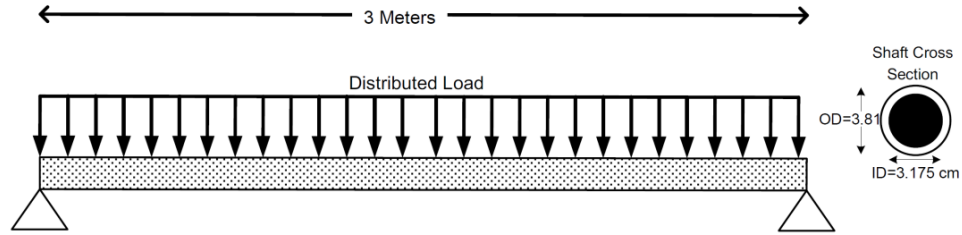


Figure 15: Turbine shaft loading regime

This loading is applied to the turbine shaft while it is rotating. The analysis is for failure due to fatigue. The first assumption made, is the type of steel that will be used for this turbine shaft. The strength properties for 1040 Hot Rolled steel will be used as this is very common steel. The ultimate strength and tensile strength (Shigley, et al., 2004 p. 994) of this steel are as follows:

$$\begin{aligned} S_{ut} &= 520MPa \\ S_y &= 290MPa \end{aligned} \quad (11)$$

For a rotating shaft, the test specimen endurance limit can be estimated by

$$S'_e = 5.04(S_{ut}) \quad (12)$$

The assumed surface condition modification factor and the size modification factor are as follows:

$$\begin{aligned} k_a &= 57.7 \\ k_b &= .84 \end{aligned} \quad (13)$$

The assumption is made that the load modification factor, the temperature modification factor, the reliability factor, and the miscellaneous effects factor are all equal to 1. The endurance limit for a shaft with can be found by

$$S_e = S'_e k_a k_b k_c k_d k_e k_f \quad (14)$$

The maximum moment for a distributed load on a beam can be found by

$$M_{max} = \frac{-qL^2}{8} \quad (15)$$

The bending stress, assuming infinite life, can be found by

$$\sigma_{inf} = \frac{M_{max}}{I/c} \quad (16)$$

Table 6 shows the values calculated for this frame analysis.

Table 6: Hollow Shaft Fatigue Analysis

Givens			Calculated Values		
Strength Ult	520	Mpa	S'_e	262.08	Mpa
Strength Yield	290	MPa	k_a	0.65	
Shaft Length	1.75	m	k_b	0.84	
Shaft Outer Diameter	1.5	in	S_e	142.80	Mpa
Shaft Inner Diameter	1.25	in	M_{max}	395.98	Nm
Shaft Outer Diameter	0.0381	m	I	5.35534E-08	
Shaft Inner Diameter	0.03175	m	I/c	2.8112E-06	
Distributed load q	1034.4	N/m	σ_{inf}	140.86	Mpa
Wind Speed	90	mph			
Wind Speed	40.2336	m/s			
Swept area	1.73	m ²			
Force Drag	1810.19	N			
Coefficient of Drag	1.28				

Because the calculated bending stress is less than that of the endurance limit, this shaft will not fail under fatigue at sustained 90mph winds.

Guy Wire Analysis

The guy wires that support the frame structure are under an axial tension loading. If the wind direction is directly in line with one of the guy wire supports, then this support will be taking the entire drag loading. The loading regime for the guy wire can be seen in Figure 16.

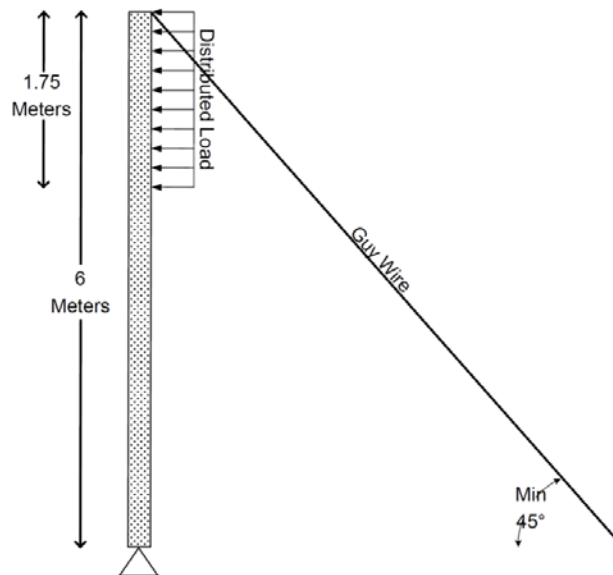


Figure 16: Guy wire loading regime

The tension force applied to the guy wire can be found by

$$F_t = \frac{F_d}{\cos(45)} \quad (17)$$

The guy wire chosen is a 3.175 mm thick steel cable with a breaking strength of 5907 N (Lexco Cable Inc). Given the constraints, the maximum calculated force of tension is 2560 N. This results in a FS of 2.3.

Chapter 6: Experimental Analysis

6.1 Testing Plan

Extensive research has been done on a majority of the system components. The one piece of information that needs to be experimentally tested is the wind turbine. Although the Savonius has been rigorously tested, power curves for this specific design need to be produced to accurately predict the flow rates from the pump. To produce power curves, the turbine torque, turbine shaft speed, and wind speed need to be measured, given that (Beer, et al., 1992)

$$P = T\omega \quad (18)$$

Because this is a full-sized turbine, testing will be done in an outdoor setting. Data will be collected over long periods of time and analyzed to find times of constant wind speed. The load was slowly increased until the turbine could no longer consistently be producing power. Power curves for four different turbine loading regimes will be produced using this method.

6.2 Experimental Setup

Data Acquisition Hardware and Software

The experimental setup required the collection of data from three different sensors to produce power curves. The individual sensors will be discussed in subsequent sections. This section details the signal conditioning hardware, data acquisition hardware and software. A one-line diagram of the data acquisition equipment can be seen in Figure 17.

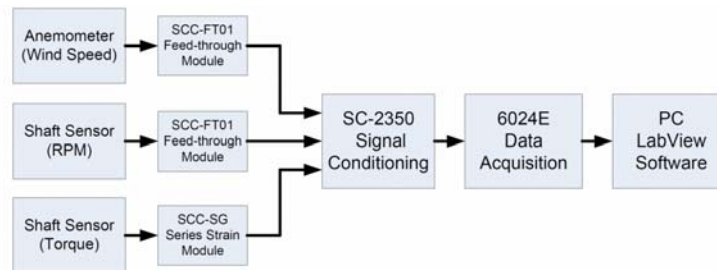


Figure 17: Data Acquisition One-line Diagram

The signal conditioning was done using a National Instruments (NI) SC-2350 Signal Conditioning with Configurable TEDS (Transducer Electronic Data Sheet) connectors. This signal conditioning board was chosen because the torque sensor was equipped with a TEDS. The NI SC-2350 can be seen in Figure 18.



Figure 18: NI SC-2350 Signal Conditioning

The data acquisition card chosen was the NI DAQ Card 6024E seen in Figure 19.



Figure 19: NI 6024E Data Acquisition Card

The NI 6024E card was chosen because the PCMCIA output is compatible with a laptop computer. This allowed the data acquisition system to be mobile. High noise levels were experienced when the laptop was charging from a square wave inverter powered from a vehicle battery. For this reason, all data was taken while the laptop was powered using the internal battery.

The software used to read and process the signals into usable data was LabVIEW 8.5. Screen shots of both the front panel and the block diagram used to read and process the signals can be seen in Figure 20 and Figure 21.

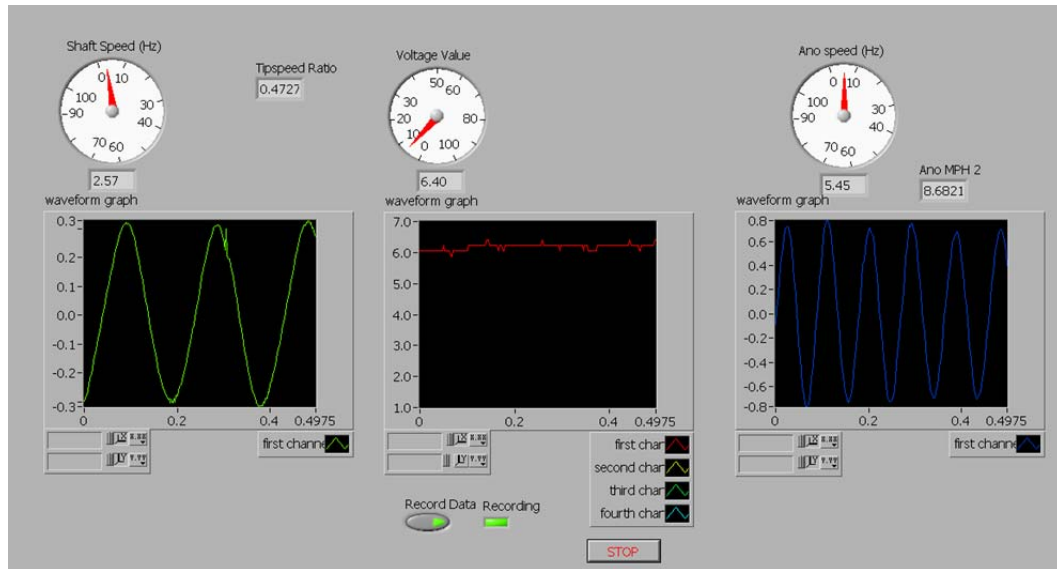


Figure 20: LabVIEW Front Panel

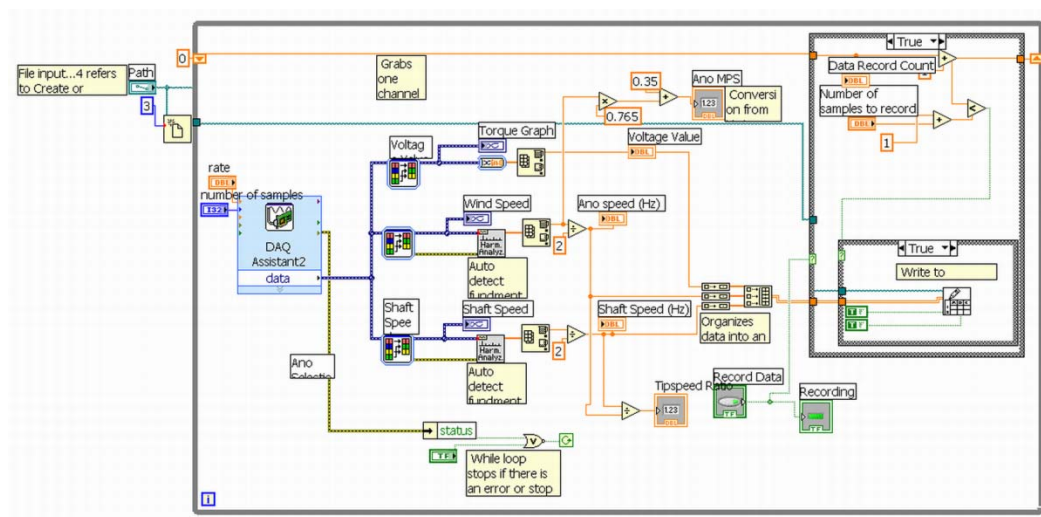


Figure 21: LabVIEW Block Diagram

Torque Measurement

The torque data was obtained with an in-line torque sensor mounted to the shaft between the shaft of the turbine, and a loading shaft. The sensor chosen was a Transducer Technique RSS Series rotating socket wrench torque sensor, depicted in Figure 22.



Figure 22: Turbine experimental setup

The torque sensor requires a 10 V excitation to power the internal full bridge strain gage. The excitation voltage is supplied by a SCC-SG Series Strain Gauge Input Module seen in Figure 23.



Figure 23: NI SCC-SG Series Strain Gauge Input Module

To ensure that the sensor is accurate over the entire range of testing, a calibration test was performed. This was done using the experimental setup shown in Figure 24.



Figure 24: Torque sensor calibration experimental setup

The setup consisted of a long steel bar that attached to the torque sensors input. Various weights were hung from the bar at various distances to load the torque sensor with known values. This method allowed a torque sensor calibration test to be performed. The static calibration data can be seen in Appendix 5 and shows that this sensor is accurate to the nearest .8 N*m for the calibration range, but accurate to the nearest .3 N*m for the range of data collected for the power curves.

With the torque sensor calibrated, the power curves for the Savonius turbine were then measured. The torque sensor was mounted at the output shaft, and a loading shaft was mounted below the torque sensor. The shaft brake (Figure 22) was then used to apply various frictional loads to the turbine shaft.

Shaft Speed Measurement

The shaft speed was measured using a modified NRG #40C calibrated anemometer. The cups were removed and the anemometer was mounted directly to the turbine loading shaft. The calibration data for this sensor can be found in Appendix 6. A photo of the sensor used can be seen in Figure 25.



Figure 25: Shaft speed sensor

The signal from the shaft speed sensor was then routed to the NI SC-2350 Signal Conditioning board via a NI SCC-FT01 feed through module seen in Figure 26.



Figure 26: NI SCC-FT01 feed through module

Wind Speed Measurement

The wind speed was measured using an NRG #40C calibrated anemometer mounted on the turbine frame at hub height. This anemometer can be seen in Figure 27.



Figure 27: NRG #40C calibrated anemometer

An additional anemometer was mounted on a wooden pole 30 m from the turbine to ensure that the wind data collected was accurate. These anemometers were connected to the SC-2350 Signal Conditioning board via a redundant NI SCC-FT01 feed through module depicted in Figure 26. To ensure accuracy, both anemometers were mounted on 1.25 m booms at 60° from the direction of the prevailing wind. Research has determined that this angle is the most accurate angle to avoid pressure differentials.(Filippelli, et al., 2005) A depiction of these pressure differentials can be seen in Figure 28.

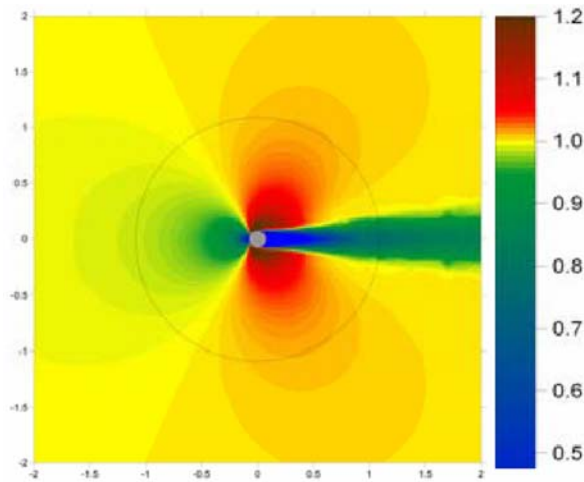


Figure 28: Computational flow analysis around a mast (Filippelli, et al., 2005)

6.3 Processing Data

Power Curves

Because the wind speeds are not constantly provided by a wind tunnel, the experimental data required processing to see specific trends. Data collected during times of transition, when wind speed is increasing or decreasing, were removed. The first step in removing wind data during these ramping periods was to calculate the standard deviation for a rolling window. This window was 10 data points, or 10 seconds wide. If the standard deviation was greater than 1 m/s within this 10 second period, then the data was removed from the sample. After the ramp data had been removed, the remained data was binned and averaged. The bin width was .05 m/s. This data was then plotted, and a third order polynomial trend line was added. Four different loading regimes were analyzed, and can be seen in Section 6.4. This process was done using MATLAB. The M-File used to process the data can be Appendix 7.

Pump Curves

Once the power curves were created, the equation for the trend line for each power curve was used to estimate the instantaneous pump flow rate. This was done for three different head values. The M-File used to build the pump curves can be found in Appendix 8. With instantaneous flow rates defined, the Rayleigh distribution was used to predict annual average flow rates. This is discussed in detail in Section 6.4. The M-File used to build the annual average flow curves can be found in Appendix 9.

6.4 Experimental Results

Turbine

The resulting power curves can be seen in Figure 29 thru Figure 32. Note that the trend lines are only valid for the range of data that is shown on the power curve. Any attempt to extrapolate beyond these limits could result in large errors.

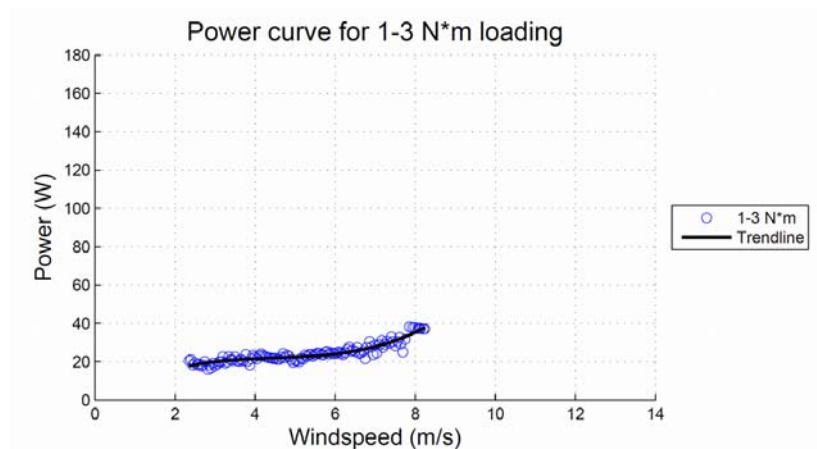


Figure 29: Power curve for 1-3 N*m loading.

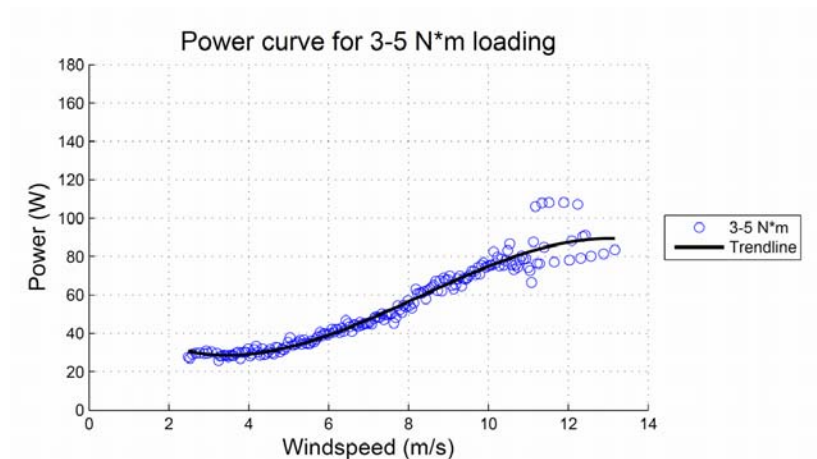


Figure 30: Power curve for 3-5 N*m loading.

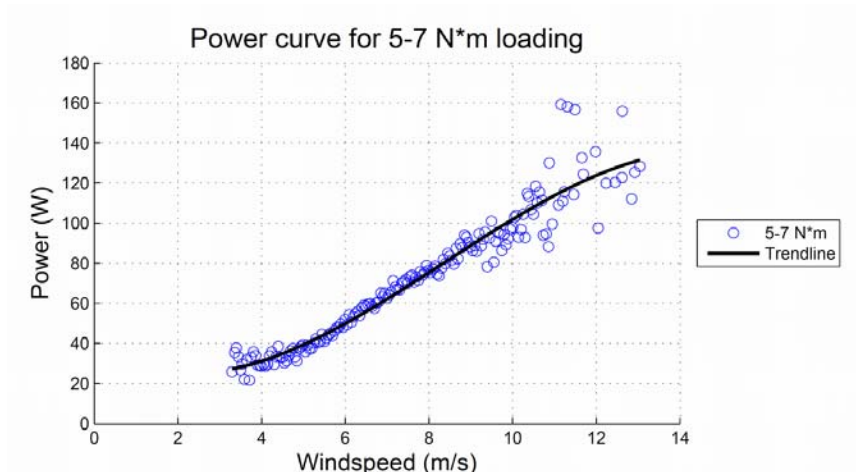


Figure 31: Power curve for 5-7 N*m loading.

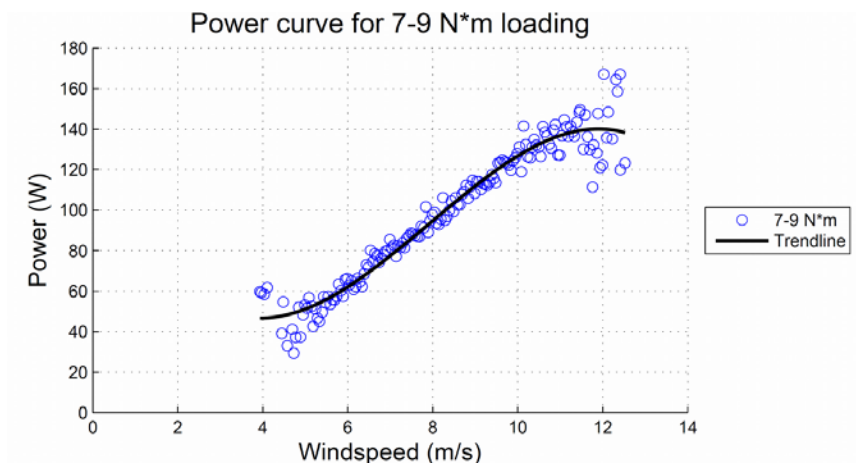


Figure 32: Power curve for 7-9 N*m loading.

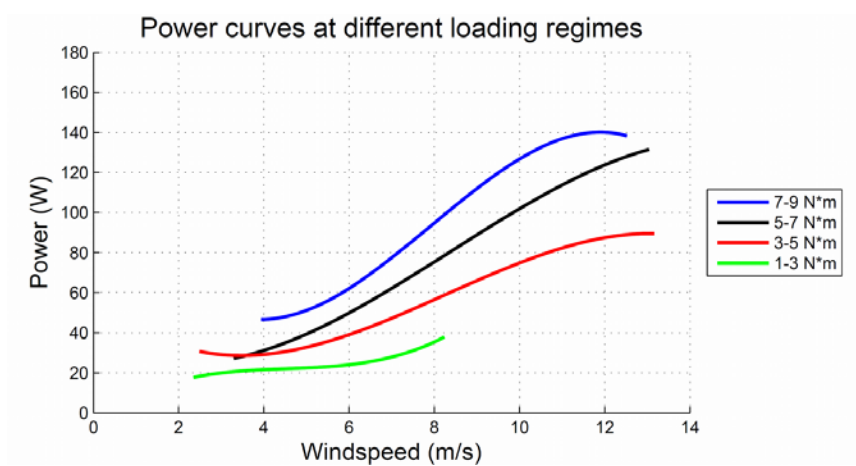


Figure 33: Summary of turbine power curves for various loadings

These power curves show how an increase in load will capitalize on available power primarily at the upper end of the power curve. This is because at lower load, the rotor spins faster. This results in higher frictional and drag losses. At higher loading the losses decrease, and more power is extracted from the wind. At loading values beyond 7-9 N*m, the turbine slows dramatically and the power drops off as the rotor does not spin consistently. This information is crucial when designing a turbine to be used for pumping. An important point to note is that the startup wind speeds for the smaller loads are lower. This makes lower loading regimes more attractive where lower annual average wind speeds are expected. The average wind speed, filter requirements, and pump efficiencies all play a part in determining the most efficient loading regime.

Now we can determine the theoretical power output for this specific turbine and compare the results. The first step in determining the theoretical power is to determine the wind power density for different wind speeds. The wind power density (WPD) can be found by (Twindell, et al., 2006)

$$WPD = \frac{1}{2} \rho V^3 \quad (19)$$

Density at sea level and 15°C is assumed to be $1.225 \frac{Kg}{m^3}$. The power coefficient for a typical Savonius rotor with no overlap can be seen in Figure 34.

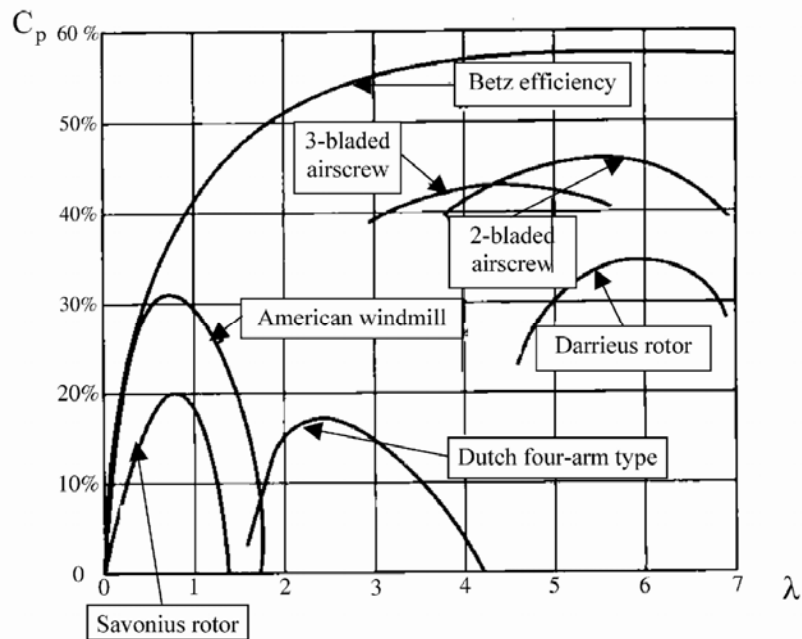


Figure 34: Performance of conventional wind turbines (Menet, 2002)

The typical Savonius rotor has a power coefficient that peaks at 20%, however, with a gap ratio of 25%, the power coefficient peaks at 28% (Sargolzaei, 2007). An average tip speed ratio of .6 is assumed resulting in an average power coefficient of 20%. The results are summarized in Table 7.

Table 7: Theoretical power output

Wind Velocity (m/s)	Available Power	Power Coefficient	Power Output (W)
1.00	0.61	20%	0.21
2.00	4.90	20%	1.70
3.00	16.54	20%	5.72
4.00	39.20	20%	13.56
5.00	76.56	20%	28.49
6.00	132.30	20%	45.78
7.00	210.09	20%	72.69
8.00	313.60	20%	108.51
9.00	446.51	20%	154.49
10.00	612.50	20%	211.93
11.00	815.24	20%	282.07
12.00	1058.40	20%	366.21

These theoretical values, assuming no losses, can then be compared to the experimentally derived power curve. This comparison can be seen in Figure 35.

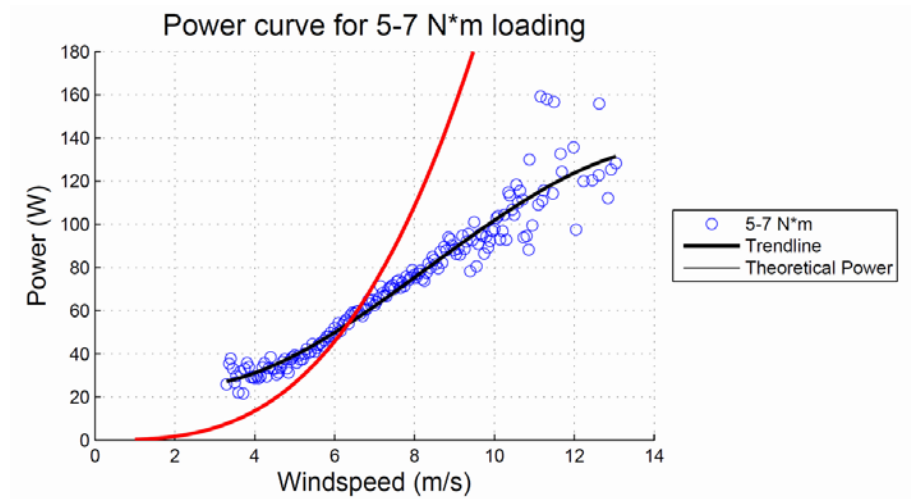


Figure 35: Collected data and predicted power

The increase in efficiency at the lower wind speeds due to the overlap ratio and the end caps can be seen in Figure 35. The data deviates from the predicted power as the wind speed increases. The predicted power was derived using a fixed tip speed ratio. This assumption gives an accurate prediction for the lower end of the power curve, but does not accurately predict power at higher wind speeds. This is because the tip speed ratio is affected by increased drag losses as the blades of the rotor start to impact the turbulent

wake of the blade proceeding. One other thing to note is that the experimental testing was done at an elevation of about 2300 m. The power curves published here would increase about 15% at sea level because the air density is higher.

Uncertainty Analysis

Before the power curves were created, an estimate of the uncertainty of the measurements and data was calculated. The uncertainty was affected by temporal variation error or data scatter, instrument error, and propagation of error to results. Calibration data for the two sensors used to calculate power can be found in Appendix 5 and Appendix 6. The largest error recorded for each of these calibration curves was used. These values were 2% of reading for the torque sensor, and 0.011 Hz or 0.069 rad/s for the shaft speed sensor.

The uncertainty of each point plotted in the power curves will have a different value. This is because the number of points in each bin will be different. Because of this reason, an uncertainty at two different points of the power curve was analyzed for comparison. These points can be seen in Figure 36.

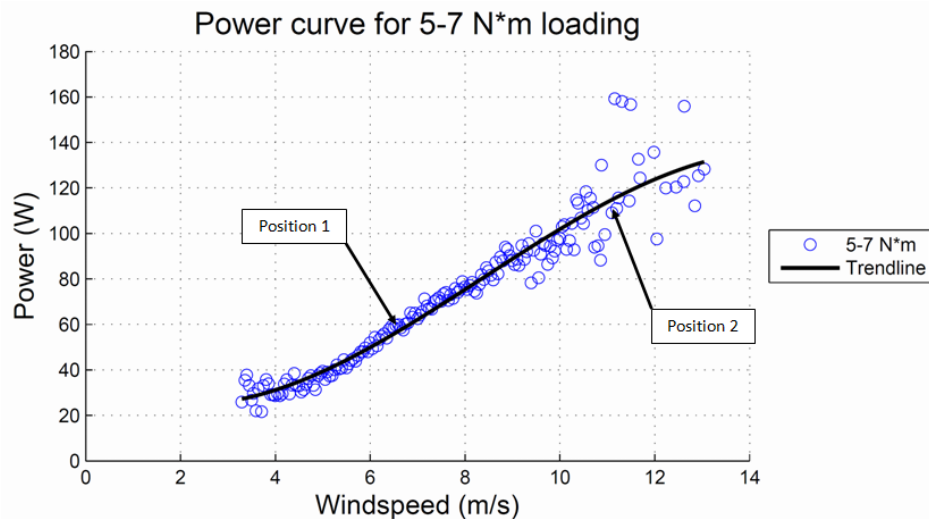


Figure 36: Uncertainty calculation points

The value at Position 1 was $58.89 \pm 2.75W$. The value at Position 2 was $104.28 \pm 45.37W$ (Figliola, et al., 2006). These uncertainty values are calculated at a 95% confidence interval. The large difference in uncertainty was influenced almost entirely by the number of data points evaluated in the bin. The bin at Position 1 had 199 data points, where the bin at Position 2 had only 20. The data scatter at the upper end of the curve is a

visual of this uncertainty. The M-File used to calculate uncertainty can be seen in Appendix 10. Calculating the uncertainty for each of the points in the power curve was not reasonable because of the sheer number of points.

Turbine and pump combined

Now that we have the power output from the turbine, and the power requirements from the pump, we can estimate pumping curves. With this information we can size a filtration system. This will also allow for proper sizing with regards to local wind speeds.

The first step in determining the pump curves is to estimate the losses from the power transfer mechanisms, and the pump losses. Keep in mind that the only factors that have not been applied in the experimental analysis of the turbine power curves are the power transfer efficiency and the pump efficiency. If the pump has been purchased, the manufacturer should supply expected efficiency. If it is a homemade pump, the efficiency can be estimated using Table 4. For the sake of consistency, all graphs and calculations in this report assume an efficiency of 60% power transfer from the turbine shaft, through the pump.

Instantaneous Flow rate

An estimation of the instantaneous flow rate can be found by (White, 2003)

$$Q = \frac{P\eta}{\rho g H_p} \quad (20)$$

Using the power curves from the turbine, the output pumping curves can be given assuming a fixed pump head H_p . If frictional losses in the pipe are neglected, the pump head is equal to the pumping height. Pumping curves for one of the loading regime power curves can be seen in Figure 37.

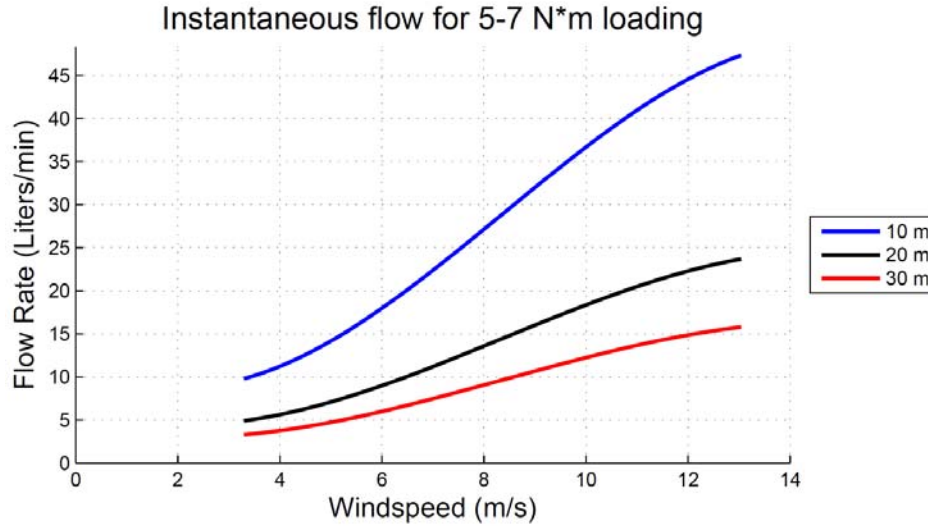


Figure 37: Instantaneous flow curve for turbine loading 5-7 N*m

Given the low annual average wind speed across much of Ghana, the pumping curve for the 5 to 7 N*m loading regime will be better suited to this system. The startup speeds for a turbine loaded at this magnitude are considerably lower, and this loading will still allow the rotor to capitalize on power production at higher wind speeds. This loading will be used for the remaining calculations.

Average Flow rate

In order to determine the average flow rate, it is necessary to know the quality of the wind resource. The distribution of the wind speed will be approximated using the Rayleigh probability density function. This function is defined by (Manwell, et al., 2002)

$$P(V) = \frac{\pi}{2} \left(\frac{V}{\bar{V}^2} \right) \exp \left(-\frac{\pi}{4} \left(\frac{V}{\bar{V}^2} \right)^2 \right) \quad (21)$$

The Rayleigh probability density function indicates the frequency at which the wind will blow at a given speed and is based solely on the average wind speed at a given site. If accurate wind data is available, the Weibull distribution can be used to provide more accurate results. Figure 38 shows the Rayleigh probability density function for four different average wind speeds.

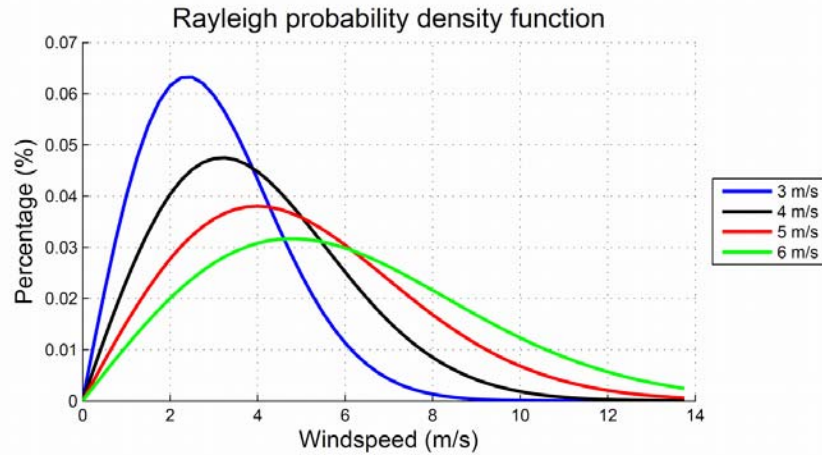


Figure 38: Rayleigh Probability Density Function at four average wind speeds

Now that there is an estimation of the wind distribution given an average wind speed, one can predict the average flow rate given an average wind speed. This is done by using the power curve regression equations, Equation (19) and Equation (20) . When this is done over a range of wind speeds, the average flow rate can be predicted. The results can be seen in Figure 39 and Table 8.

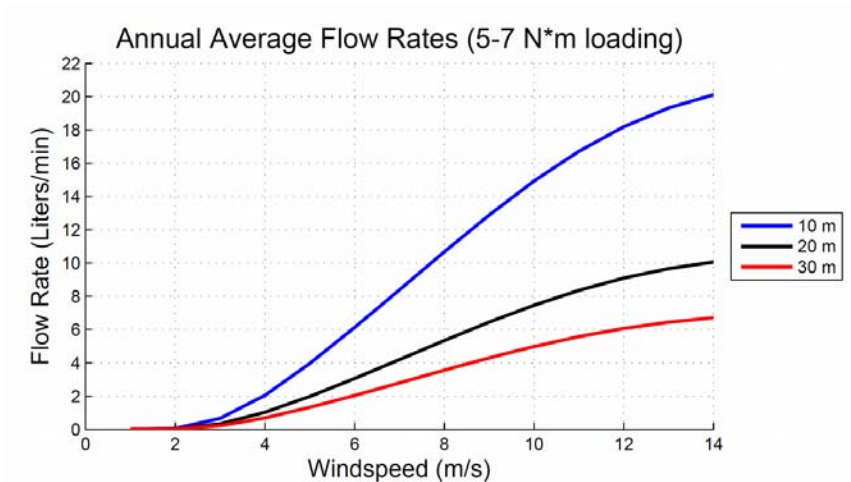


Figure 39: Annual average flow rates VS annual average wind speeds

Table 8: Daily average flow rates (lit/day) VS annual average wind speed

Average Wind Speed (m/s)	10 meters	20 meters	30 meters
1	89	44	30
1.5	517	258	173
2	944	472	315
2.5	1,945	972	649
3	2,945	1,472	982
3.5	4,323	2,161	1,441
4	5,701	2,850	1,900
4.5	7,259	3,630	2,420
5	8,817	4,409	2,939
5.5	10,450	5,225	3,483
6	12,082	6,041	4,027
6.5	13,725	6,862	4,575
7	15,367	7,683	5,122
7.5	16,959	8,480	5,653
8	18,551	9,276	6,184

The World Health Organization estimates that the required daily water usage for drinking and cooking per person is 7.5 liters (World Health Organization, 2003). With this information, and the results in Table 8, the number of people that can be supported by this system can be estimated. The annual wind average of the area that Engineers Without Borders is working in Ghana is 3.5 m/s, and the average well is 10 m deep, thus this system can provide water to over 575 people.

Chapter 7: Journal Article Submission

7.1 Journal Manuscript

The venue selected for publication, was the Energy for Sustainable Development published by Elsevier. This journal focuses on energy issues in developing countries. Findings from the research presented in this thesis that are applicable to this topic have been put together and submitted for publication. A copy of the manuscript submitted can be found in Appendix 11.

Chapter 8: Conclusions

8.1 Combined system overview

An example of what a complete system might look like, including water storage, can be seen in Figure 40.



Figure 40: Complete water treatment system including storage

The drums directly under the rotor represent pre-filter storage on top of a parallel BSSF, while the blue drums represent post-filter storage. In this specific configuration, the post filter storage is used to cap the shallow well.

8.2 Design Requirements Results

Qualitative Requirements

Simple

Appropriate technology was selected. Operations and maintenance processes are simple, and with training, anyone can operate this system.

Reliable

With parallel filters, the reliability of this system is increased as no downtime is required for routine maintenance. Every part of the system is designed from simple, locally available parts, to increase reliability.

Affordable

The estimated upfront cost for this system is \$520.75 with a monthly maintenance cost of \$11. This breaks down to \$0.91 per person for the upfront cost, and \$.02 per person per month. A complete bill of materials, with prices can be found in Appendix 12.

Sustainable

The affordable system cost, locally available materials, independent power source, and simple operation all qualify this solution as sustainable.

Effective

The effectiveness of the water treatment meets global and local water quality standards for raw water faecal coliform concentration up to 1400/100ml sample.

Quantitative Requirements

Contaminants

With a design requirement of faecal coliform levels of raw water not exceed 300/100 ml sample, the expected levels of the water output is 2.1/100 ml sample. This far exceeds the maximum value of 10/100 ml allowed.

Flow Rates

The flow rates for this system will provide water for up to 575 people. The system can be custom sized to meet requirements for anywhere from 50-575 people.

Pump Head

This solution is designed to pump water anywhere from 10 to 40 meters. Pump selection should take into consideration the target pump head.

Weather

The system exceeds expectations, and operates in weather similar to Ghana. The system could even be successful at sites with average wind speeds as low as 3 m/s.

Robust

Components selected for this solution are designed to be robust, and designed to last a minimum of one year.

This solution addresses the problem of purifying contaminated surface water, with a system that is simple, reliable, affordable, sustainable, and effective.

Works Cited

- Bailey, Peter N. 2007.** *Demand Analysis and Optimization of Renewable Energy: Sustainable Rural Electrification of Mbanayili, Ghana.* 2007. p. 100.
- Beer, Ferdinand P. and Johnston Jr., Russell E. 1992.** *Mechanics of Materials .* 2nd Edition. New York : McGraw-Hill, 1992.
- Borger, Michael, et al. 2005.** *Mae Nam Khun Thailand Clean Drinking Water Project Report.* s.l. : EWB-Cal Poly SLO, 2005. p. 44.
- Brace Research Institute. 1973.** *How to Construct a Cheap Wind Machine for Pumping Water.* Quebec : Brace Research Institute, 1973. p. 5.
- CAWST. 2009.** *Biosand Filter Manual.* Alberta : Centre for Affordable Water and Sanitation Technology, 2009. p. 2.
- DIY Trade.** Pillow block ball bearings. [Online] [Cited: 12 8, 2010.] http://www.diytrade.com/china/4/products/2733627/pillow_block_ball_bearing.html.
- Figliola, Richard S and Beasley, Donald e. 2006.** *Theory and Design for Mechanical Measurements 4e.* Hoboken NJ : John Wiley & Sons, Inc, 2006.
- Filippelli, Matthew and Mackiewicz, Pawel. 2005.** *Experimental and Computational Investigation of Flow Distortion Around a Tubular Meteorological Mast.* Ontario : CanWEA Conference, 2005.
- Fraenkel, P.L. 1986.** *Water Lifting Devices.* Rome : Food and Agricultural Organization of the United Nations, 1986. pp. 137-138,240.
- Global Spec.** Bracket flange bearing housing. [Online] [Cited: 12 8, 2010.] http://www.globalspec.com/industrial-directory/bracket_flange_bearing_housing.
- Green, David W., Winandy, Jerrold E. and Kretschmann, David E. 1999.** *Mechanical Properties of Wood.* Department of Agriculture. Madison : Forest Products Laboratory, 1999. pp. 4-7, Technical Report.
- Huisman, L. and Wood, W.E. 1974.** *Slow Sand Filtration.* Geneva : World Health Organization, 1974. p. 22.
- Kaeding Performance.** Radius rods and Rod ends. [Online] [Cited: 12 9, 2010.] http://www.kaedings.com/index.php?main_page=index&cPath=45.
- Lexco Cable Inc.** Aircraft Cable. *LexcoCable.* [Online] [Cited: May 5, 2010.] http://www.lexcocable.com/7x19_aircraft_cable.html.

Lidia, Canepa de Vargas. *Slow Filtration as Disinfectant.*

Manwell, J F, Mcgowan, J G and Rogers, A L. 2002. *Wind Energy Explained.* Sussex : J Wile and sons, 2002.

Menet, J. L. 2002. *A double-step Savonius rotor for local production of electricity: a design study.* s.l. : Elsevier, 2002. p. 7.

Muhammad, Nur. 1996. *Optimization of slow sand filtration.* 1996. pp. 1-2.

Sargolzaei, J. 2007. *Prediction of the power ratio and torque in wind turbine Savonius rotors using artificial neural networks.* 2007. p. 12.

Shigley, Joseph E., Mischke, Charles R. and Budynas, Richard G. 2004. *Mechanical Engineering Design.* New York : Mc Graw Hill, 2004.

Twindell, John and Weir, Tony. 2006. *Renewable Energy Resources.* New York : MPG Books LTD, 2006.

U.S. Department of Energy. 2004. *Ghana 50m Wind Power.* s.l. : National Renewable Energy Laboratory, 2004.

United Nations Environment Programme Global Environment Monitoring System. 2007. *Global Drinking Water Quality Index Development and Sensitivity Analysis Report.* Ontario : United Nations Environment Programme Global Environment Monitoring System (GEMS)/Water Programme, 2007. p. 10.

Ushiyama, I and Nagai, H. 1988. *Optimum design configurations and performances of Savonius rotors.* 1988. pp. 59-75.

White, Frank M. 2003. *Fluid Mechanics.* 5th edition. New York : McGraw-Hill, 2003. pp. 747-751.

World Health Organization. 2010. 10 Facts about water scarcity. *World Health Organization.* [Online] May 22, 2010. [Cited: May 22, 2010.] <http://www.who.int/features/factfiles/water/en/>.

World Health Organization. 2003. *Domestic Water Quantity.* Geneva : World Health Organization, 2003. p. 15.

World Health Organization. 2009. *World Health Statistics.* s.l. : World Health Organization, 2009. p. 83.

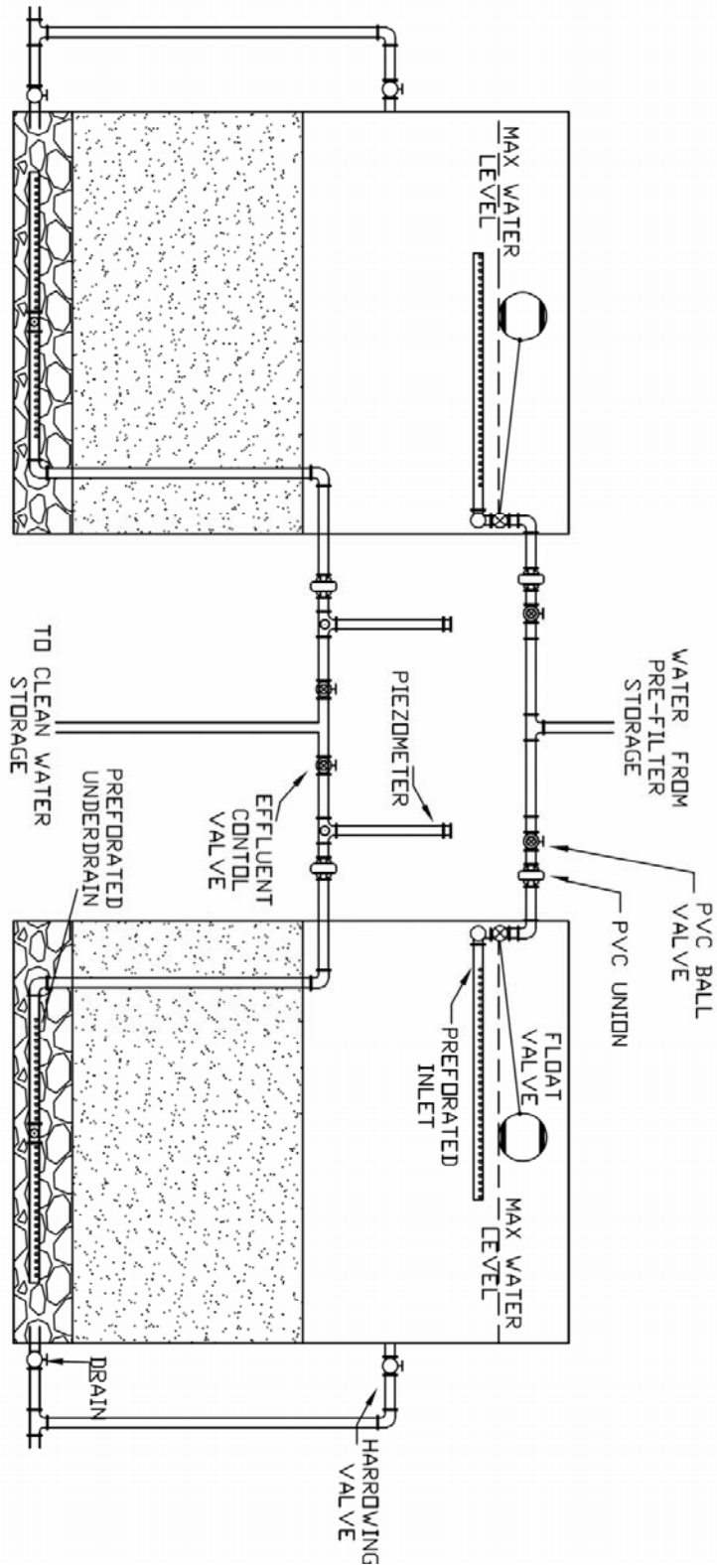
Appendices

Appendix 1: Unlined well water quality data

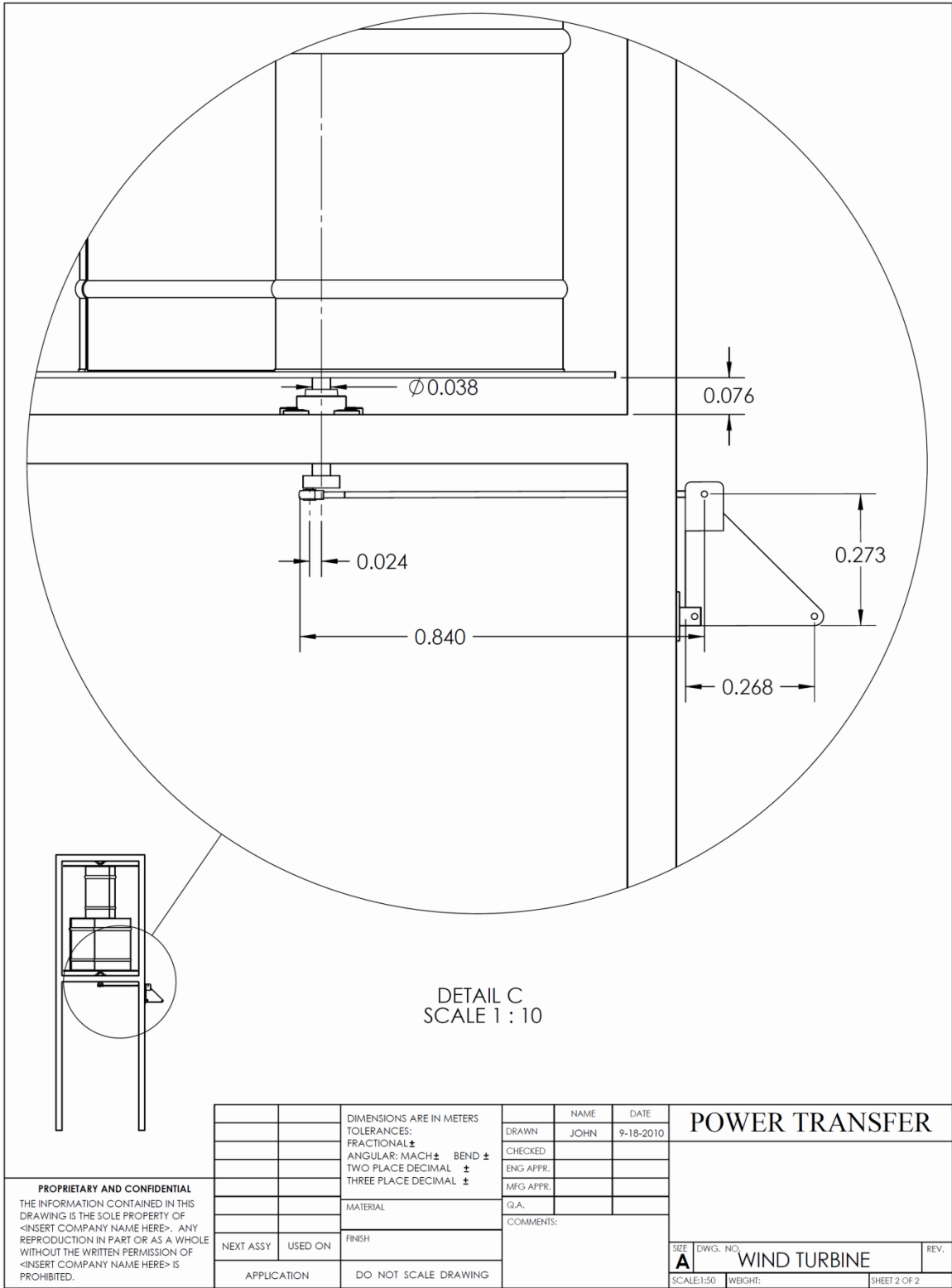
Water Quality Data Northern Ghana Summer 2009

Parameter	Unit	Spillway	Unlined Well	Bore Hole (1)	WHO Guideline
Turbidity	NTU	123	65.4	1.43	5
Color (apparent)	Hz	20	10	< 2.50	15
Odor	-	-	-	-	Inoffensive
pH	pH Units	6.8	6.9	6.83	6.5-8.5
Conductivity	µS/cm	39.3	195	366	-
Tot. Susp. Solids (SS)	mg/l	180	36	< 1.00	-
Tot. Dis. Solids (TDS)	mg/l	21.6	107	201	1000
Sodium	mg/l	3.5	21.8	24.8	200
Potassium	mg/l	2.8	2.2	2.9	30
Calcium	mg/l	2.4	13.6	29.7	200
Magnesium	mg/l	1.9	7.3	17	150
Total Iron	mg/l	3.04	2.89	0.098	0.3
Ammonium (NH ₄ -N)	mg/l	0.009	< 0.001	< 0.001	
Chloride	mg/l	2	6	13.9	250
Sulphate (SO ₄)	mg/l	3.2	18.9	5.48	400
Phosphate (PO ₄ -P)	mg/l	0.353	0.597	0.521	-
Manganese	mg/l	0.087	0.158	< 0.005	0.5(P)
Nitrite (NO ₂ -N)	mg/l	0.061	0.084	< 0.001	-
Nitrate (NO ₃ -N)	mg/l	1.09	7.38	1.39	10
Total Hardness	mg/l	14	64	144	500
Total Alkalinity	mg/l	18	70	158	-
Calcium Hardness	mg/l	6	34.1	74.1	-
Mag. Hardness	mg/l	8	29.9	69.9	-
Fluoride	mg/l	< 0.005	0.191	< 0.005	1.5
Bicarbonate	mg/l	21.9	85.4	193	-
Carbonate	mg/l	0	0	0	-
Fecal Coliform	#/100ml	360	40	0	10
Non-Fecal Coliform	#/100ml	167000	6000	0	-

Appendix 2: Plumbing for parallel filters



Appendix 4: Power transfer drawing



Appendix 5: Torque sensor calibration data

Torque Sensor Calibration Data							
Distance (in)	Weight (grams)	Bar Torque (ft*lbs)	Total Torque (ft*lbs)	Measured Torque (down)	Difference	Measured Torque (up)	Difference
6	546	7.5415	8.143	8.388	-0.245	8.3	-0.157
24	546	7.5415	9.949	10.118	-0.169	10.12	-0.171
30	546	7.5415	10.551	10.723	-0.172	10.72	-0.169
42	546	7.5415	11.754	11.934	-0.180	11.93	-0.176
48	546	7.5415	12.356	12.539	-0.183	12.54	-0.184
24	1546	7.5415	14.358	14.358	0.000	14.44	-0.082
30	1546	7.5415	16.062	16.062	0.000	16.09	-0.028
36	1546	7.5415	17.766	17.766	0.000	17.81	-0.044
42	1546	7.5415	19.471	19.471	0.000	19.46	0.011
48	1546	7.5415	21.175	21.175	0.000	21.19	-0.015
42	2046	7.5415	23.329	23.329	0.000	23.35	-0.021
48	2046	7.5415	25.584	25.52	0.064	25.51	0.074
42	2546	7.5415	27.187	27.187	0.000	27.15	0.037
48	2546	7.5415	29.993	29.933	0.060	29.993	0.000
42	3046	7.5415	31.045	31.1	-0.055	31.02	0.025
48	3046	7.5415	34.403	34.165	0.238	34.165	0.238
48	3546	7.5415	38.812	38.289	0.523	38.289	0.523
42	4649	7.5415	43.414	43.414	0.000	43.414	0.000
48	4649	7.5415	48.539	48.539	0.000	48.539	0.000
30	6929	7.5415	45.731	45.713	0.018	45.731	0.000
36	6929	7.5415	53.369	53.369	0.000	53.369	0.000
42	6929	7.5415	61.007	61.007	0.000	61.573	-0.566
48	6929	7.5415	68.645	68.837	-0.192	68.645	0.000

Max	0.523	Max	0.523
Average	-0.013	Average	-0.031
Min	-0.245	Min	-0.566

Appendix 6: Shaft speed sensor calibration data

anno speed (Hz)	motor speed (Hz)	Abs Val Difference
2.345	2.343	0.002
2.346	2.348	0.002
2.342	2.341	0.001
2.341	2.34	0.001
2.348	2.348	0
2.352	2.353	0.001
2.352	2.35	0.002
2.357	2.358	0.001
2.357	2.358	0.001
2.353	2.354	0.001
2.351	2.35	0.001
2.352	2.352	0
2.348	2.35	0.002
2.35	2.348	0.002
2.348	2.347	0.001
2.347	2.35	0.003
2.344	2.341	0.003
2.339	2.338	0.001
2.339	2.342	0.003
2.343	2.342	0.001
2.342	2.341	0.001
2.344	2.348	0.004
4.985	4.985	0
4.982	4.982	0
4.993	4.993	0
4.995	4.995	0
5.002	5.002	0
5.003	5.003	0
5.005	5.005	0
5.001	5.001	0
4.999	4.999	0
4.997	4.997	0
4.998	4.997	0.001
4.993	4.992	0.001
4.989	4.989	0
4.992	4.991	0.001
4.999	4.998	0.001
5.002	5.002	0
5	4.999	0.001
5.005	5.005	0
4.998	4.997	0.001
4.996	4.995	0.001
4.991	4.99	0.001
4.994	4.994	0
7.611	7.61	0.001
7.606	7.606	0
7.604	7.603	0.001
7.605	7.604	0.001
7.597	7.596	0.001
7.603	7.603	0

7.599	7.599	0
7.589	7.589	0
7.596	7.596	0
7.596	7.596	0
7.585	7.584	0.001
7.573	7.573	0
7.58	7.58	0
7.576	7.576	0
7.588	7.587	0.001
7.59	7.59	0
7.588	7.589	0.001
7.588	7.588	0
7.599	7.599	0
7.599	7.598	0.001
7.606	7.606	0
10.23	10.23	0
10.229	10.229	0
10.229	10.229	0
10.233	10.232	0.001
10.213	10.211	0.002
10.191	10.19	0.001
10.215	10.215	0
10.201	10.201	0
10.204	10.203	0.001
10.195	10.195	0
10.172	10.171	0.001
10.18	10.18	0
10.189	10.19	0.001
10.166	10.166	0
10.183	10.183	0
10.166	10.166	0
10.179	10.179	0
10.186	10.186	0
10.19	10.19	0
10.187	10.186	0.001
10.216	10.215	0.001
10.214	10.214	0
12.831	12.831	0
12.829	12.829	0
12.825	12.826	0.001
12.843	12.843	0
12.837	12.837	0
12.831	12.831	0
12.838	12.838	0
12.833	12.832	0.001
12.836	12.836	0
12.839	12.839	0
12.84	12.84	0
12.839	12.838	0.001
12.828	12.828	0
12.83	12.83	0

12.833	12.833	0
12.831	12.831	0
12.827	12.828	0.001
12.832	12.831	0.001
12.834	12.833	0.001
12.825	12.825	0
12.833	12.832	0.001
12.017	12.017	0
15.466	15.466	0
15.486	15.486	0
15.458	15.458	0
15.47	15.47	0
15.46	15.459	0.001
15.487	15.487	0
15.471	15.471	0
15.496	15.496	0
15.468	15.467	0.001
15.461	15.461	0
15.475	15.476	0.001
15.485	15.485	0
15.483	15.483	0
15.491	15.49	0.001
15.487	15.487	0
15.482	15.482	0
15.486	15.486	0
15.488	15.488	0
15.482	15.482	0
15.489	15.489	0
15.489	15.49	0.001
15.489	15.49	0.001
18.079	18.078	0.001
18.089	18.089	0
18.099	18.099	0
18.113	18.113	0
18.103	18.103	0
18.118	18.118	0
18.089	18.089	0
18.091	18.09	0.001
18.109	18.109	0
18.099	18.099	0
18.107	18.107	0
18.091	18.091	0
18.094	18.094	0
18.098	18.097	0.001
18.091	18.091	0
18.1	18.1	0
18.097	18.097	0
18.097	18.097	0
18.104	18.104	0
18.11	18.11	0
18.099	18.098	0.001

25.911	25.911	0
25.923	25.922	0.001
25.923	25.921	0.002
25.929	25.931	0.002
25.916	25.915	0.001
25.952	25.952	0
26.007	26.007	0
25.981	25.98	0.001
25.986	25.979	0.007
25.999	25.994	0.005
25.994	25.99	0.004
25.978	25.976	0.002
25.951	25.949	0.002
25.972	25.97	0.002
25.968	25.968	0
25.961	25.964	0.003
25.957	25.956	0.001
25.974	25.974	0
25.948	25.946	0.002
25.953	25.955	0.002
25.968	25.969	0.001
25.979	25.98	0.001

Max Difference 0.011

Appendix 7: Data Processing M-File

9/19/10 10:01 AM C:\Users\jcampbell\Documents\MATLAB\DataProcessRev2.m

1 of 3

```
%-----Double-Step Savonius Rotor Data Processor-----  
%-----  
% clc  
% clear  
C1 = 3.28084; %Ft/m  
C2 = 4.448222; %N/lbf  
[FileName,PathName,FilterIndex]- uigetfile;  
FileLocation =[PathName FileName];  
M=dlmread(FileLocation);  
  
F = M(:,1)*C2/C1; %Torque in N*m  
W = ((M(:,2))*2*0.765)+0.35; %Wind Speed in m/s  
S = (M(:,3))*2*pi; %Shaft Speed in Rad/sec  
P=F.*S; %Calculate Power  
STATS = [F W S P]; %Place variables into one vector  
  
NumPts=20; %Number of Points for Rolling  
L = length(W); %Find number of points  
  
%-----Rolling Averaging of Torque -----  
FA=[];  
for x = 1:L-NumPts  
    data1=F(x:x+(NumPts-1));  
    average1 = sum(data1)/NumPts;  
    FA=[FA;average1];  
end  
  
%-----Rolling Averaging of Shaft Speed -----  
SA=[];  
for x = 1:L-NumPts  
    data1=S(x:x+(NumPts-1));  
    average1 = sum(data1)/NumPts;  
    SA=[SA;average1];  
end  
  
%-----Rolling Averaging of Wind Speed -----  
WA=[];  
for x = 1:L-NumPts  
    data1=W(x:x+(NumPts-1));  
    average = sum(data1)/NumPts;  
    WA=[WA;average];  
end  
  
%-----Rolling Standard Deviation of Wind Speed -----  
SD=[];  
for x = 1:L-NumPts  
    data1=W(x:x+(NumPts-1));  
    SDvar = std(data1);  
    SD=[SD;SDvar];  
end
```

```

%-----Rolling Power -----
PA=[];
for x = 1:L-NumPts
    data=STATS(x:x+(NumPts-1),4);
    PAVar = sum(data)/NumPts;
    PA=[PA;PAVar];
end

%-----Combine Rolling Averages into one matrix-----
ROLL=[FA WA SD PA];

%-----Wind Speed Ramp Remover-----
PCData=[];
SDLimit=1;
L2=length(WA);
for x = 1:L2-NumPts
    if ROLL(x,3)<SDLimit; %Checks that Standard Dev
        PCData=[PCData;ROLL(x+NumPts,:)]; %is below the limit
    end
end

%-----Select Loading regime-----
LowerLimit=7; %Limit in Newtons
UpperLimit=9;

DataSel=[];
B=sortrows(PCData,1);
L3=length(B);
for x=1:L3
    if B(x,1)<UpperLimit && B(x,1)>LowerLimit;
        DataSel=[DataSel;B(x,:)];
    end
end

%-----Step Wise Power -----
PAF=[];
PowerTemp=[];
WFLog=[];
PFLog=[];
L4=length(DataSel);
DataSel=sortrows(DataSel,2);
%scatter(DataSel(:,2),DataSel(:,4))
space=.05;

for y=min(DataSel(:,2)):space:max(DataSel(:,2))
    WindTemp=[];
    for x = 1:L4
        if DataSel(x,2)<(y+space) && DataSel(x,2)>y;
            WindTemp=[WindTemp;DataSel(x,:)];
        end
    end
end

```

```
end
if length(WindTemp)>1
WF=mean(WindTemp(:,2));
WFLog=[WFLog;WF];
FF=mean(WindTemp(:,4));
FFLog=[FFLog;FF];
end
end
WAT=[];

scatter(WFLog,FFLog)

%-----PolyFit-----
p=polyfit(WFLog,FFLog,3);
f=polyval(p,WFLog);
hold on
plot(WFLog,f,'k','LineWidth',2);

%-----Plot Information-----
title('Power curve for 7-9 N*m loading','fontsize',16)
legend('7-9 N*m','Trendline','Location','EastOutside')
xlabel('Windspeed (m/s)','fontsize',14);
ylabel('Power (W)','fontsize',14);
axis([0 14 0 180])
grid
```

Appendix 8: Pump Curve M-File

9/20/10 8:44 AM C:\Users\jcampbell\Documents\MATLAB\PumpCurve.m 1 of 1

```
%-Pumping Curves
PumpEff=.6;
leng=length(f);
PumpCurveTemp=[];
PumpCurveVel=[];

for n=10:10:30          %10 20 and 30 meters of head
    for i=1:leng
        temp=f(i)*PumpEff/10000/n*264.172052*60/0.264172;
        PumpCurveTemp=[PumpCurveTemp;temp];
    end
    PumpCurveVel=[PumpCurveVel,PumpCurveTemp];
    PumpCurveTemp=[];

end
hold on
plot(WFLog,PumpCurveVel(:,1),'b','LineWidth',2);
plot(WFLog,PumpCurveVel(:,2),'k','LineWidth',2);
plot(WFLog,PumpCurveVel(:,3),'r','LineWidth',2);

%-----Plot Information-----
title('Pump Curve for 5-7 N^m loading','fontsize',16)
legend('10 m','20 m','30 m','Location','EastOutside')
xlabel('Windspeed (m/s)','fontsize',14);
ylabel('Flow Rate (Liters/min)','fontsize',14);
axis([0 14 0 (max(PumpCurveVel(:,1))+1)])
grid
```

Appendix 9: Annual Average Flow M-File

9/20/10 8:47 AM C:\Users\jcampbell\Documents\MATLAB\AnnualAverage.m 1 of 2

```
%Annual Average Flow Rate

PumpEff=.6;

Distribution=[];
delta=WFLog(3)-WFLog(2);
WSpeed=[0:.25:14];
WSpeed=transpose(WSpeed);
leng=length(WSpeed);
FlowRate=[];

for Wind=1:.5:8
Distribution=[];

    for i=1:leng-1
        temp=(pi()/2)*(WSpeed(i)/(Wind^2))*exp((-pi()/4)*(WSpeed(i)/Wind)^2)*(WSpeed^(i+1)-WSpeed(i));
        Distribution=[Distribution;temp];
    end

leng=length(f);
PumpCurveTemp=[];
PumpCurve1=[];
p=polyfit(WFLog,PFLog,3);
f=polyval(p,WSpeed);
leng=length(f);
for x=10:10:30
    for i=1:leng
        temp=f(i)*PumpEff/10000/x*264.172052*60/0.264172;
        PumpCurveTemp=[PumpCurveTemp;temp];
    end
    PumpCurve1=[PumpCurve1,PumpCurveTemp];
    PumpCurveTemp=[];
end
AnnualAveTemp=[];
for i=1:leng-1
    temp=Distribution(i)*3600*365*PumpCurve1(i,3);
    AnnualAveTemp=[AnnualAveTemp;temp];
end
Ray=[WSpeed(1:leng-1) Distribution AnnualAveTemp PumpCurve1(1:leng-1,1)]
SumVec=[];

for i=1:leng-1
    r=Ray(i)
    if r >= 4
        temp=[Ray(i,:)]
        SumVec=[SumVec;temp];
    end
end
AnAve=sum(SumVec(:,3))/(3600*365);
FlowRate=[FlowRate;AnAve]
```

```
end
hold on
%plot(WFLog,PumpCurvel(:,3),'r','LineWidth',2);
plot(FlowRate,'r','LineWidth',2)

title('Annual Average Flow Rates','fontsize',16)
legend('10 m','20 m','30 m','Location','EastOutside')
xlabel('Windspeed (m/s)','fontsize',14);
ylabel('Flow Rate (Liters/min)','fontsize',14);
axis([0 (14) 0 (22)])
grid
```

Appendix 10: Uncertainty M-File

9/21/10 10:40 PM

Untitled

1 of 2

```

for y=min(DataSel(:,2)):space:max(DataSel(:,2))
    WindTemp=[];
    for x = 1:L4
        if DataSel(x,2)<(y+space) && DataSel(x,2)>y;
            WindTemp=[WindTemp;DataSel(x,:)];
        end
    end
    if length(WindTemp)>1
        WF=mean(WindTemp(:,2));
        WFLog=[WFLog;WF];
        PF=mean(WindTemp(:,5));
        PFLog=[PFLog;PF];
        %ROLL=[FA WA SD SA PA];
        % average Force Average wind average Shaft
        % 1Average Torque 2 Average wind 3average Shaft 4std Torque
5std Shaft 6 number of Data points
        Un=[mean(WindTemp(:,1)),mean(WindTemp(:,2)),mean(WindTemp(:,4)),std(WindTemp(:,1)),
std(WindTemp(:,4)),length(WindTemp)];
        UnSave=[UnSave;Un];
    end
end
WAF=[];

%%-----Uncertainty Calculation-----
for x=51

    Et=.03*UnSave(x,1);
    Es=.069115;
    Et=UnSave(x,4)/sqrt(UnSave(x,6));
    Es=UnSave(x,5)/sqrt(UnSave(x,6));
    EP= sqrt( (UnSave(x,1)*Ps)^2 + (UnSave(x,3)*Et)^2 );
    BP= sqrt( (UnSave(x,1)*Bθ)^2 + (UnSave(x,3)*Et)^2 );

    v= ( sqrt( (UnSave(x,1)*Ps)^2 + (UnSave(x,3)*Pt)^2 ) ) / ( ( (UnSave(x,1)
*Ps)^4)/UnSave(x,6) + ( (UnSave(x,3)*Pt)^4)/UnSave(x,6) );
    if v<1
        t=12.7
    elseif v<2
        t=4.3
    elseif v<3
        t=2.7
    elseif v>3 && v<7
        t=2.5
    else
        t=2.2
    end
    UPower=sqrt((BP^2)+((t*EP)^2))
end

```

Appendix 11: Elsevier Journal Submission

Adaptable Wind-Powered Filtration System for Rural Water Treatment

Thomas L. Acker Ph.D.^a, John Tester Ph.D.^a, John C. Campbell^b, Mathew Acker^c

- a. *Professor of Mechanical Engineering, Northern Arizona University*
- b. *MS Candidate The Graduate School Department of Mechanical Engineering, Northern Arizona University*
- c. *BS Candidate Department of Mechanical Engineering Northern Arizona University*

Corresponding Author:

Name:	John Campbell
Permanent Address	15220 N 2 nd St Phoenix AZ: 85022 United States
Phone Number	001(802)993-5889
Email Address	johncharlescampbell@gmail.com

Abstract

Sustainable, low-cost water treatment systems are critical elements to developing nations and remote off-grid areas of the developing world. According to the World Health Organization, water and sanitation are the primary drivers of public health. This research will build on proven theory and technology to develop an adaptable, affordable and sustainable system for treating drinking water in off-grid rural environments. Components of this design will be analyzed and tested for application in rural Africa through an Northern Arizona University (NAU) Engineers Without Borders (EWB) Student Chapter project in Ghana. An annual average wind speed of 3.5 m/s at a height of three meters is assumed with surface water fecal bacteria levels not exceeding 300/100 ml sample. The system is designed to use readily available, low-cost materials and renewable wind energy to treat contaminated surface waters in order to make clean drinking water more accessible to communities in need. The design chosen utilizes a Savonius rotor used in conjunction with a positive displacement pump to move water through a biological slow sand filter. Power curves for a specified Savonius rotor design are found experimentally and allow for estimation of the water treatment system output. Results indicate that this system will be able to provide clean drinking water for up to 575 people.

Nomenclature

A_{piston}	area of the piston (m^2)
d	diameter of each rotor scoop (m)
D	diameter of rotor (m)
d_{10}	Effective grain size
D_f	diameter of end plates (m)
e	gap between main paddles: main overlap
F	force (N)
F_x	force in the x axis (N)
F_y	force in the y axis (N)
g	acceleration of gravity
h	height of water (meters)
H	bell crank height (m)
H_p	pump head (m)
L	bell crank length (m)
N	Newton
NTU	Nephelometric Turbidity Units
P	power (Watts)
P_{fluid}	pressure of the fluid (Pascals)
Q	volumetric flow rate (m^3/s)
T	torque ($\text{N}\cdot\text{m}$)
U	sand grain uniformity coefficient
V	wind Velocity (m/s)
\bar{V}	average wind velocity (m/s)
W	work (joules)
β	overlap ratio
Δd	displacement (m)
η	pumping efficiency (%)
ρ	fluid density (kg/m^3)
ω	angular velocity (rad/s)

1.0 Introduction

"Close to a billion people are still without access to improved water supplies, half of whom live in the African and Western Pacific Regions" (World Health Organization, 2009). This results in 41% of the people in Africa having no access to clean water. This same report indicates that the majority of the 41% are from lower income families located in rural areas. This creates engineering design constraints that are quite challenging. Most often, unimproved surface water is available, but this water usually contains harmful contaminants. Water sources like these are scattered across northern Ghana, and are prevalent throughout underdeveloped areas of the world. Working in northern Ghana with the Northern Arizona University (NAU) Engineers Without Borders (EWB) Chapter, it was discovered that a large majority of people use water from sources such as these for drinking. The effects of consuming water of this quality causes a myriad of health issues. "Poor water quality can increase the risk of such diarrheal diseases as cholera, typhoid fever and dysentery, and other water-borne infections." (World Health Organization, 2010)

Biological slow sand filtration (BSSF) has been used in rural settings and has proven itself as an appropriate technology for conditions found in Africa. "No other single process can effect such an improvement in the physical, chemical and bacteriological quality of surface waters" (Huisman, et al., 1974). BSSF utilizes both physical and biological treatment of water. Physical treatment is an effect of mechanical filtration, and the biological treatment is a result of the development of a biological layer on the top layer of sand (Muhammad, 1996). This biological layer will be referred to as a biofilm.

The discovery of the effectiveness of BSSF in intermittently operated filtration has led to its widespread use. This allows the filter to be loaded with contaminated water on an as needed basis. In the past, most slow sand filters required continuous operation, because it was believed that the biofilm must be constantly supplied with both oxygen and a food source. Perceptions changed as lab results showed that the biofilm could be supplied with oxygen through diffusion if the water level is held just above the biofilm. This has led to the use of small household water treatment filters. These household filters can be scaled up to provide water for larger families or communities.

Moving water through biological slow sand filters requires energy. In a rural setting, where electricity isn't available, options for moving water are limited. Because the flow rates required for BSSF are relatively low, it becomes challenging to consistently keep the filter manually loaded. It can become a full time job to constantly add water to the filter. The design solution proposed here utilizes a wind powered pump to keep water constantly moving through the filter

and producing clean water. For the windmill¹, a Savonius turbine has been selected, as displayed in Figure 1.



Figure 1: A practical Savonius windmill and tower (Brace Research Institute, 1973).

A Savonius wind turbine was selected for this application due to its low start-up speed, high torque characteristics, and its ability to function in areas with low to moderate wind resources. In this design, the rotor is built from two 55 gallon oil drums (or similar drums available locally). The structure (tower) upon which the rotor will be mounted elevates the base of the rotor approximately 3 meters above the ground, as depicted in Figure 1. The tower is designed to be built out of wood, creating a fairly ridged structure, with concrete footers at the base. Guy wires made of a 3.175 mm thick galvanized steel cable support the structure.

Addressing the problem of purifying contaminated surface water requires a water purification system that is simple, reliable, affordable, sustainable, and effective. A system utilizing a Savonius wind turbine as the prime mover and BSSF for water treatment has been selected. The purpose of this report is to detail the design of such a system.

¹ A "windmill" is a wind powered device that produces mechanical energy for grinding or pumping, etc. This is distinguished from the modern use of the phrase "wind turbine" which is generally taken as a wind powered device that produces electricity.

2.0 Materials and methods

2.1 Water treatment system design

The design for the filter system is comprised of three components, pre-filter storage, biological slow sand filters, and post-filter storage. In the event of the surface water being highly turbid (greater than 50 NTU), a roughing filter can be added as a fourth component. This prevents premature clogging of the filters. A one-line diagram showing how water flows through these components can be seen in Figure 2.

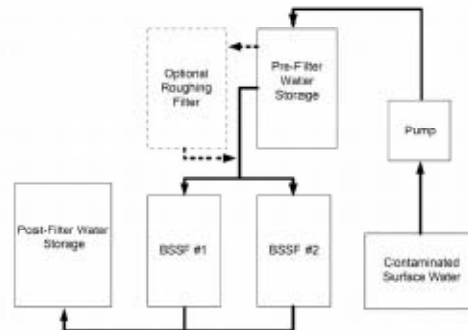


Figure 2: Water treatment system one-line diagram.

To increase the cost effectiveness of the solution, each of the system components will utilize 55 gallon drums. Polypropylene drums are preferred over steel drums, as they are more resistant to corrosion. This design selection allows the system to be modular. If the post-filter storage size must be increased, another drum can be added. In this way, a system can be sized to meet specific design requirements.

Because filter cleaning requires downtime, during which it is desirable to have continued access to clean water, the design places two filters in parallel. This allows one filter to be cleaned, while the other can remain in operation. A diagram of the plumbing layout for the parallel biological slow sand filters is provided in Figure 3.

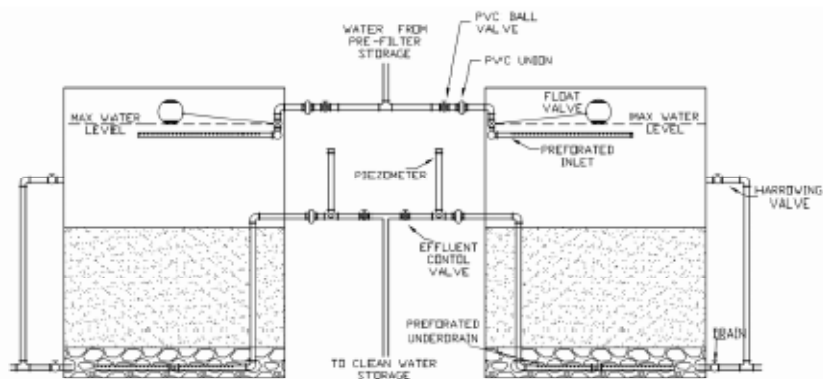


Figure 3: Plumbing and tanks for parallel biological slow sand filters (Borger, et al., 2005).

The effective grain size and uniformity coefficient play important roles in the removal rates for a BSSF. The effective grain size d_{10} is defined as the value at which 10% of the grains are smaller, and 90% of the grains are larger. This can be found using a sieve analysis.

The uniformity coefficient is defined by

$$U = \frac{d_{60}}{d_{10}} \quad (1)$$

Here, d_{60} is found in a manner similar to d_{10} but 60% of the grains are smaller, and 40% of the grains are larger. Figure 4 shows how these values can be found when graphing the results of a sieve analysis.

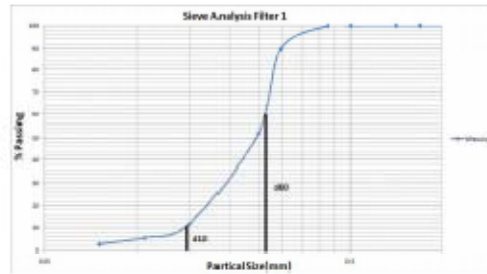


Figure 4: Typical results from a sieve analysis.

Because these factors affect removal, an effective grain size of .35 mm with a uniformity coefficient of 2 has been chosen to standardize this design. These parameters were selected to allow extended filter runtime between cleanings, while maintaining adequate removal rates (Muhammad, 1996).

The depth of the sand does affect the removal rates, but not drastically. Research has shown that a sand bed depth of 45 cm is sufficient for the target

faecal coliform removal rates of 99% (Muhammad, 1996). The filter is constructed from a drum. The drum should be filled with 50 centimeters of filter sand, sieved to the correct effective size and uniformity coefficient. During cleaning, some sand may be removed. When the sand level reaches 45 cm, more sand should be added.

Flow rates for BSSF can have a dramatic affect on the removal rates. Low flow rates increase removal rates, but if flow rates become too high, the likelihood of decreased removal rates and parasitic breakthroughs increases. For this reason, the filter has been designed to operate at or below 1m/hr once the biofilm layer has fully developed. The volumetric flow rate can be found using this linear flow rate by multiplying by the cross sectional area of the filter. The cross sectional area of a standard 55 gallon drum will require an average flow rate of 5.65 liters per minute to keep the filter constantly loaded. With the grain size, uniformity coefficient, and flow rate determined, Table 1 shows the estimated removal rates for faecal coliform, total coliform, turbidity and color.

Table 1: Experimentally derived removal rates for BSSF (Muhammad, 1996).

Filtration Rate (m/hr)	Average % Removal			
	FC	TC	Turbidity	Colour
0.1	99.60	99.70	96.50	95.10
0.2	98.70	98.90	90.10	93.80
0.3	98.30	98.10	89.10	89.60

With these removal rates, this treatment system can treat raw water with a faecal coliform concentration of up to 1400/100ml sample, and still stay below the maximum allowable concentration of 10/100ml sample (United Nations Environment Programme Global Environment Monitoring System, 2007). As the filter becomes clogged, the flow rates will decrease. When the flow rate drops below an acceptable level, the filter must be cleaned. .

Because the flow rates for BSSF are relatively slow, pre-filter storage and post-filter storage allows the system to treat water continuously and meet demand for a reliable clean water supply. Proper sizing of these storage tanks will ensure successful system operation. Pre-filter storage allows water that is pumped during higher wind speeds to be stored, and processed by the filters when wind speeds are lower. The lower the average wind speed, the larger your pre-storage requirement. Assuming a distribution of wind speeds described by the Rayleigh distribution (explained in detail in the results section) one can predict the amount of time that the pump will be providing water at a flow rate larger than the filter can process. The pre-filter storage should be sized using the percentage that the pump will be providing less than the filter can process. This value applied by the hourly flow rate will give an estimate of the cushion provided by the pre-filter storage. Post-filter storage allows water that is processed to be stored before being used. This is especially important, as water processed at night can be used

during the day. To store all the water that has been pumped during the night, half of the daily flow will be required for storage. This may result in a very large post-filter storage, and decisions on storage size need to be balanced with cost.

Although BSSF is a simple process, there are certain precautions that must be taken to ensure that the system effluent is maintained at a satisfactory level. The first step in ensuring that this takes place is allowing adequate time for the biofilm to develop. This is done by letting the filter operate at the design flow rate. The rate at which the biofilm will develop varies as a function of influent water quality and temperature. During this time, water from the filter should not be used. When the biological layer has developed, testing of the raw water and from the effluent should be taken to verify that the filter is performing at the desired removal rates. This process can take two weeks to a month.

Once the biofilm has developed, the filter can be operated at the design flow rate. The flow rate should be monitored, and adjusted using the effluent control valve shown in Figure 3. When the flow rate drops below .5 m/hr the filter has become clogged, and will need to be cleaned. With two filters operating in parallel as shown in Figure 3, one filter can be cleaned while the other remains in service. The cleaning process that will allow the filter to be down the least amount of time is a process called "wet harrowing". This requires the effluent control valve to be closed. The filter is then filled with water and the surface is agitated by swirling the water manually. Water is then removed by opening the harrowing valve. This process is repeated until a significant amount of biomass has been removed from the filter. This process is one of the easiest maintenance procedures for slow sand filters and allows the biofilm to redevelop in about seven days. Before the filter is placed back into service, testing from the raw water and from the effluent should be taken to verify that the filter is performing at the desired removal rates.

2.2 Pump selection

This system is designed to use a positive displacement pump. With this in mind, a pump that has locally available replacement parts, or can be constructed with locally available material should be selected. Table 2 shows some pump selection parameters.

Table 2: Typical parameters for positive displacement pumps (Fraenkel, 1986).

Pump Type	Head Range (m)	Input Power (kW)	Flow Range (m ³ /h)	Efficiency (%)
Piston/Bucket pumps	5-200+	.03-50+	2-100+	40-85
Plunger pumps	40-400	.50-50+	2-50+	60-85
Diaphragm pumps	1-2	.03-5	2-20	20-30

With these values in mind, pump diameter, pump stroke, pump head, and cost should all be taken into consideration when selecting a pump. An example of

sizing a pump to a specific turbine loading target can be found in the turbine design section and may assist in pump selection.

2.3 Savonius Turbine Design

The rotor is designed to be built out of two steel or polypropylene barrels that are cut in half and then mounted on plywood end-plates. When designing a Savonius rotor, there are several geometric variables that can be changed. These variables can drastically change the performance of the rotor. Figure 5 shows these variables.

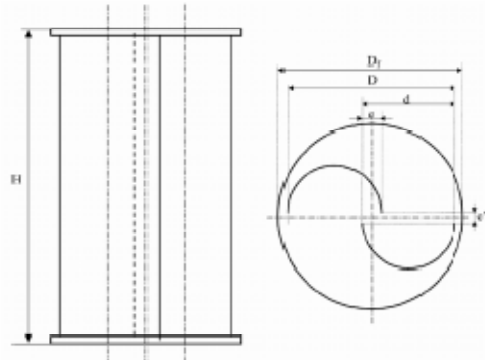


Figure 5: Design variables for a Savonius rotor (Menet, 2002).

The overlap ratio is one of the most influential design parameters of the Savonius rotor and is defined as

$$\beta = \frac{e}{d} \quad (2)$$

The variables e and d can be found in Figure 5. After extensive wind tunnel testing, it was determined that the most efficient overlap is between 20% and 30% (Menet, 2002). With this in mind, the design selected calls for an overlap ratio of 25%. With a rotor made from a standard steel, or polypropylene barrel, this overlap is 22 cm. End-plates have also proven to increase the efficiency of a Savonius rotor. It has been shown that a value of D_f 10% greater than D provides the most efficient increase in performance with the least amount of material (Ushiyama, et al., 1988). Lastly, the rotor has been designed to be a "double step" rotor. This means that the top half and the bottom half will be offset by 90°. This will provide a more efficient rotor as well as higher and more consistent start up torques (Ushiyama, et al., 1988). This will require a plate in between the upper half and the lower half of the rotor. Figure 6 depicts an example of what this rotor might look like.



Figure 6: Example of a double-step Savonius rotor.

One of the most important hardware requirements for this design is the bearings that allow the turbine shaft to rotate. These bearings are crucial to the success of the wind turbine. Bearings for the turbine must be rated to carry a 3500 N thrust load. The bearings must also be rated as self-aligning. As the turbine experiences high winds, the frame will shift. Self-aligning bearings have the ability to rotate within a socket, and prevent the bearings from experiencing unnecessary loading. These bearings can be found as pillow block bearings and flange mount bearing as can be seen in Figure 7 and Figure 8. Both mounting styles can be used.



Figure 7: Pillow block bearing(DIY Trade, 2010)



Figure 8: Flange Mounted bearing (Global Spec, 2010)

Another crucial hardware requirement is the use of rod-ends for all of the power transfer junctions. The design calls for three. The first connects the eccentric to the connecting rod, the second connects the connecting rod to the bell crank, and the third connects the bell crank to the pump rod as seen in Figure 10. These rod-ends allow for critical rotation in the linkage, as well as reduce the power transfer losses. The rating required will be determined by the maximum force occurring in the power transfer mechanisms. An example of a rod-end is displayed in Figure 9.



Figure 9: Rod-end (Kaeding Performance)

The power transfer mechanism, which changes the rotational output of the Savonius rotor to the reciprocating motion used by the pump, is illustrated in Figure 10.

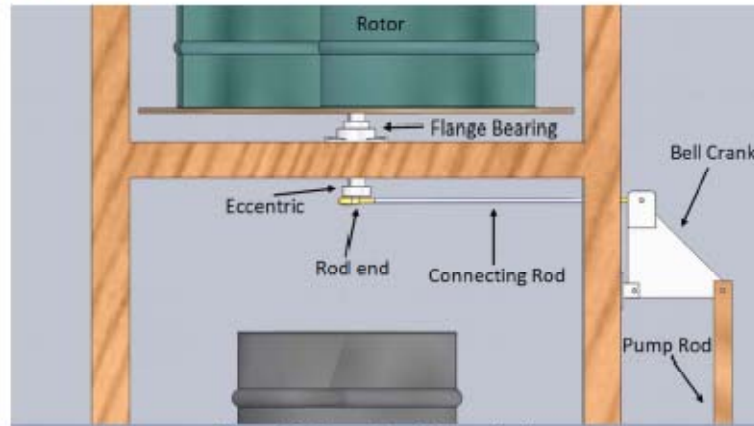


Figure 10: Power transfer mechanism

The power transfer system consists of the eccentric, the connecting rod, the bell crank, and the pump rod. These pieces work together to transfer power from the turbine shaft to the pump. The power transfer components are designed to match the desired turbine loading with a specific pump. The radius of the eccentric should be kept small compared to the diameter of the turbine. The larger the radius of the eccentric, the larger the angle between the connecting rod and the turbine frame. To reduce this angle, the eccentric radius should be no larger than 1/10 the turbine radius. A ratio of 1/20 has been chosen simply because a small piece of bar stock can be welded along the side of the turbine shaft. The connecting rod should have a threaded section to allow for adjustment in length. The length of the connecting rod should be such that when the eccentric is at its furthest position from the bell crank, the vertical section of the bell crank is parallel to the frame. The bell crank dimensions can be adjusted to change the power transfer ratio from the connecting rod to the pump rod. The ratio of distance traveled per stroke, $\Delta x/\Delta y$ is directly proportional to the ratio of the bell crank, H/L as seen in Figure 11.

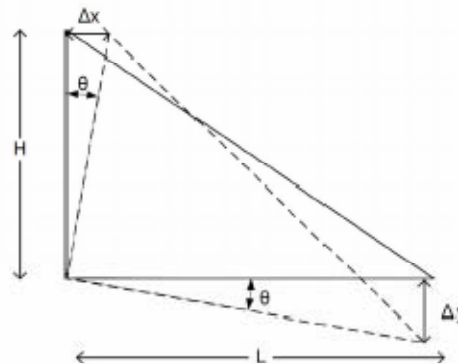


Figure 11: Bell crank distance traveled ratio.

The bell crank allows the designer the ability to change both the pumping stroke, and the pumping force. Take for example, a piston pump with a diameter of 5 cm and 15 meters of pump head. The pressure that must be applied to the piston to overcome the water pressure is found by

$$P_{\text{fluid}} = \rho gh \quad (3)$$

With the given parameters, this results in a pressure of about 148 kPa. With the force on the piston found by

$$F = P_{\text{fluid}} A_{\text{piston}} \quad (4)$$

For the given parameters, this results in a force on the piston in the y axis of about 289 N. Let's assume that the required turbine loading is 6 N*m. With an eccentric diameter to turbine diameter ratio of approximately 1/20, the radius of the eccentric is 2.38 cm or .0238 m. Dividing the turbine loading by the moment arm (radius) of the eccentric provides the target force on the connecting rod of about 252 N. Given that

$$W = F\Delta d \quad (5)$$

The conservation of work through the bell crank determines that

$$\frac{H}{L} = \frac{F_x}{F_y} \quad (6)$$

With these values we can determine the correct ratio for the bell crank. For this example a bell crank with an H/L ratio of .87 will provide the target loading of the turbine.

2.4 Experimental Analysis

The one piece of information that needed to be experimentally tested was the wind turbine rotor. Although the Savonius has been rigorously tested, power curves for this specific design needed to be produced to accurately predict the flow rates from the pump. To produce power curves the turbine torque, rotational speed, and wind speed needed to be measured given that

$$P = T\omega \quad (7)$$

Because this is a full-sized turbine, testing was done in an outdoor setting. Data was collected over long periods of time and analyzed to find times of constant wind speed. A frictional load was then applied to vary the load to the turbine using a shaft brake. Power curves for four different turbine loading regimes were produced using this method. The torque data was obtained with an in-line torque sensor mounted to the shaft between the shaft of the turbine, and a shaft brake displayed in Figure 12.



Figure 12: Experimental setup for Savonius rotor data collection.

To ensure that the sensor is accurate over the entire range of testing, a calibration test was performed. The results of this experiment showed that this sensor is accurate to the nearest $.8 \text{ N}\cdot\text{m}$ for the calibration range, but accurate to the nearest $.3 \text{ N}\cdot\text{m}$ for the range of data collected for the power curves. With the torque sensor calibrated, the power curves for the Savonius turbine were then measured. The torque sensor was mounted at the output shaft, and a loading shaft was mounted below the torque sensor. The wind speed was measured using a calibrated anemometer, and the shaft speed was measured using a modified anemometer body attached to the rotor shaft.

3.0 Results

3.1 Turbine power curves

The turbine was loaded at different values. The data was then binned and averaged and the resulting power curves are depicted in Figure 13 thru Figure 16. Note that the regression equations are only valid for the range of data that is shown on the power curve. Any attempt to extrapolate beyond these limits could result in large errors. Note that the power uncertainty is approximately $\pm 5\%$ for a 95% confidence interval between 4 and 9 m/s. Outside this range, the uncertainty increases. The loading ranges for each power curve are shown in the legend. The loading ranges were selected from a small load and increased until the rotor could not consistently produce power.

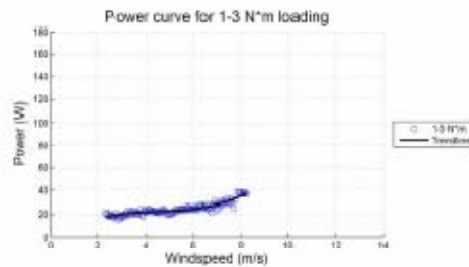


Figure 13: Power Curve 1-3 N*m

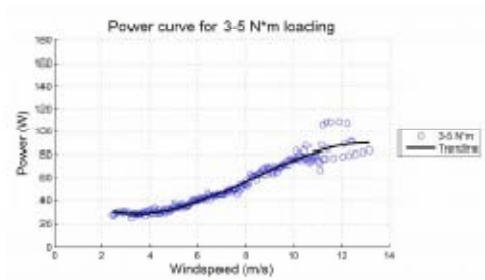


Figure 14: Power Curve 3-5 N*m

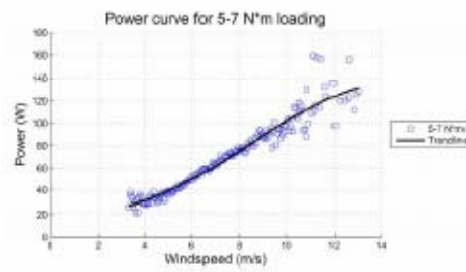


Figure 15: Power Curve 5-7 N*m

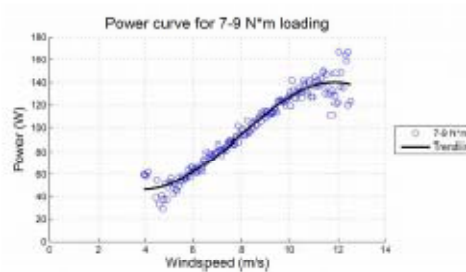


Figure 16: Power Curve 7-9 N*m

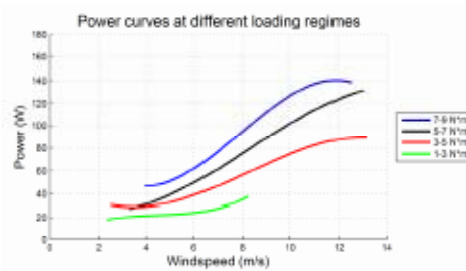


Figure 17: Summary of turbine power curves for various loadings

These power curves show how an increase in load will capitalize on available power primarily at the upper end of the power curve. This is because at lower load, the rotor spins faster. This results in higher frictional and drag losses. At higher loading the losses decrease, and more power is extracted from the wind. At loading values beyond 7-9 N*m, the turbine slows dramatically and the power drops off as the rotor does not spin consistently. This information is crucial when designing a turbine to be used for pumping. An important point to note is that the startup wind speeds for the smaller loads are lower. This makes lower loading regimes more attractive where lower annual average wind speeds are expected.

The average wind speed, filter requirements, and pump efficiencies all play a part in determining the most efficient loading regime.

3.2 Turbine and pump combined

Now that we have the power output from the turbine, and are able to determine the power requirements for a pump, we can estimate pumping curves. With this information we can size a filtration system. This will also allow for proper sizing with regards to local wind speeds. The first step in determining the pump curves is to estimate the losses from the power transfer mechanisms, and the pump losses. Keep in mind that the only factors that have not been applied in the experimental analysis of the turbine power curves are the shaft-to-pump efficiency and the pump efficiency. If the pump has been purchased, the manufacturer should supply expected efficiency. If it is a homemade pump, the efficiency can be estimated using Table 2. The power transfer losses can be kept to a minimum with the use of rod-ends and are estimated at 95% (Fraenkel, 1986). For the sake of consistency, all graphs and calculations in this report assume an efficiency of 60% power transfer from the turbine shaft, through the pump.

An estimation of the instantaneous flow rate can be found by (White, 2003)

$$Q = \frac{P\eta}{\rho g H_p} \quad (8)$$

Using the power curves from the turbine, the output pumping curves can be determined assuming a fixed pump head H_p . If frictional losses in the pipe are neglected, the pump head is equal to the pumping height. Pump curves for one of the loading regime power curves can be seen in Figure 18.

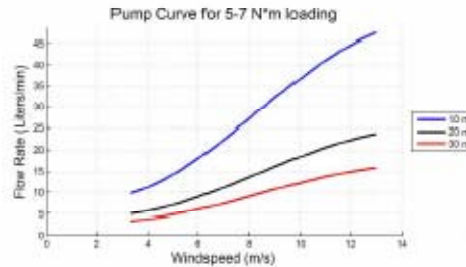


Figure 18: Instantaneous Pumping Curve for 5 to 7 N*m loading

Given the low annual average wind speed across much of Ghana, the pumping curve for the 5 to 7 N*m loading regime will be better suited to this system. The startup speeds for a turbine loaded at this magnitude are considerably lower, and this loading will still allow the rotor to capitalize on power production at higher wind speeds. This loading will be used for the remaining calculations.

In order to determine the average flow rate, it is necessary to know the quality of the wind resource. The distribution of the wind speed will be approximated using

the Rayleigh probability density function. This function is defined by (Marwell, et al., 2002)

$$P(V) = \frac{\pi}{2} \left(\frac{V}{\bar{V}^2} \right) \exp \left(-\frac{\pi}{4} \left(\frac{V}{\bar{V}^2} \right) \right) \quad (9)$$

The Rayleigh probability density function indicates the frequency at which the wind will blow at a given speed and is based solely on the average wind speed at a given site. If accurate wind data is available, the Weibull distribution can be used to provide more accurate results. Figure 19 shows the Rayleigh probability density function for four different average wind speeds.

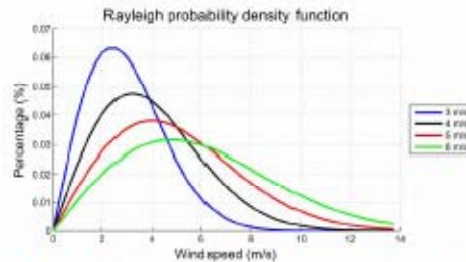


Figure 19: Rayleigh Probability Density Function for four different average wind speeds

With an estimate of the wind distribution, given an average wind speed, one can predict the average flow rate given an average wind speed. By using the power curve regression equations and Equation (8), one can compute the flow rate corresponding to each wind speed and subsequently the average flow rate over the year. The results are shown in Figure 20 and Table 3. Note that these results are for the 5 to 7 N*m loading regime.

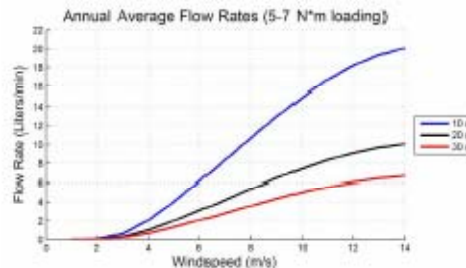


Figure 20: Annual average flow rates VS annual average wind speeds

Table 3: Daily average flow rates (liters per day) VS annual average wind speed

Average Wind Speed (m/s)	10 meters	20 meters	30 meters
1	89	44	30
1.5	517	258	173
2	944	472	315
2.5	1,945	972	649
3	2,945	1,472	982
3.5	4,323	2,161	1,441
4	5,701	2,850	1,900
4.5	7,259	3,630	2,420
5	8,817	4,409	2,939
5.5	10,450	5,225	3,483
6	12,082	6,041	4,027
6.5	13,725	6,862	4,575
7	15,367	7,683	5,122
7.5	16,959	8,480	5,653
8	18,551	9,276	6,184

The World Health Organization estimates that the required daily water usage for drinking and cooking per person is 7.5 liters (World Health Organization, 2003). With this information, and the results in Table 3, the number of people that can be supported by this system can be estimated. The annual wind average of the area that Engineers Without Borders is working in Ghana is 3.5 m/s, and the average well is 10 m deep, thus this system can provide water to over 575 people.

3.2 System Cost

A detailed bill of materials and system cost is provided in Table 4.

Table 4: Bill of materials and cost

Initial System Cost				
	#	Description	Item Cost	Cost
Turbine and Tower	2	Turbine bearings	\$45.00	\$90.00
	2	4x4 Plywood 1/2in thick	\$15.00	\$30.00
	3	4x4 Joists	\$10.00	\$30.00
	2	4x4 20ft long	\$8.00	\$16.00
	1	4x4 8ft long	\$5.00	\$5.00
	100	# 18 Galvanized Cable	\$0.40	\$40.00
	12	Wire loop ends	\$0.50	\$6.00
	12	Wire Crips	\$0.50	\$6.00
	3	1/4 Turnbuckle 4ft long	\$4.00	\$12.00
	1	Hardware	\$13.00	\$13.00
	1	7" 8000 gage 1 1/4" ID	\$5.00	\$5.00
	1	Paint	\$10.00	\$10.00
		Subtotal		\$253.00
Pump	2	1" one-way valve (steel)	\$2.50	\$5.00
	2	1" nipples (steel)	\$2.00	\$4.00
	2	1" Elbows (steel)	\$2.00	\$4.00
	1	Misc steel parts	\$10.00	\$10.00
	1	Welding Cost	\$20.00	\$20.00
		Subtotal		\$43.00
Slow Sand Filter	20	1 1/2" PVC pipe	\$0.50	\$10.00
	3	90° elbows	\$10.00	\$30.00
	1	Tube of Silicone Sealant	\$5.00	\$5.00
	8	1" PVC Ball valves	\$6.00	\$48.00
	3	1" X style PVC joint	\$1.50	\$4.50
	10	1" PVC elbows	\$0.25	\$2.50
	2	Flair valves	\$15.00	\$30.00
5	1" PVC straight joints	\$0.25	\$1.25	
		Subtotal		\$139.75
Water Storage	8	24 drums	\$10.00	\$80.00
	1	Tube of Silicone Sealant		\$5.00
		Subtotal		\$85.00
		Grand Total		\$520.75
Maintenance cost				
	#	Description	Cost per month	
	1	Lubrication	\$1.00	
	1	Misc Replacement parts	\$10.00	
		Total Monthly Cost		\$11.00

The estimated upfront cost for this system is \$520 with a monthly maintenance cost of \$11. This breaks down to \$0.91 per person for the upfront cost, and \$0.02 per person per month. Even in the most impoverished areas of the world, this cost would be considered affordable.

4.0 Conclusions

An example of what a complete system might look like, including water storage is illustrated in Figure 21.



Figure 21: Complete water treatment system including storage

The drums directly under the rotor represent pre-filter storage, and BSSF, while the blue drums represent post-filter storage. In this specific configuration, the post filter storage barrels are used to keep contaminants and people from falling into the shallow well.

The qualitative and quantitative system requirements are addressed by this design solution as follows:

- The affordable system cost, locally available materials, independent power source, and simple operation all qualify this solution as sustainable.
- The effectiveness of the water treatment meets global and local water quality standards for raw water faecal coliform concentration up to 1400/100ml sample.
- With a design requirement of faecal coliform levels of raw water not exceed 300/100 ml sample, the expected levels of the water output is 2.1/100 ml sample. This far exceeds the maximum value of 10/100 ml allowed.
- The flow rates for this system will provide water for up to 575 people. The system can be custom sized to meet requirements for anywhere from 50-575 people.
- The system exceeds expectations, and operates in weather similar that found in rural Ghana. The system could even be successful at sites with average wind speeds as low as 3 m/s.

5.0 Works Cited

- Borger, Michael, et al. 2005. *Mae Nam Khun Thailand Clean Drinking Water Project Report*. s.l. : EWB-Cal Poly SLO, 2005.
- Brace Research Institute. 1973. *How to Construct a Cheap Wind Machine for Pumping Water*. Quebec : Brace Research Institute, 1973. p. 5.
- DIY Trade. 2010. Pillow block ball bearings. [Online] 12 8, 2010. [Cited: 12 8, 2010.] http://www.diytrade.com/china/4/products/2733627/pillow_block_ball_bearing.html.
- Fraenkel, P.L. 1986. *Water Lifting Devices*. Rome : Food and Agricultural Organization of the United Nations, 1986. pp. 137-138,240.
- Global Spec. 2010. Bracket flange bearing housing. [Online] 12 8, 2010. [Cited: 12 8, 2010.] http://www.globalspec.com/industrial-directory/bracket_flange_bearing_housing.
- Huisman, L. and Wood, W.E. 1974. *Slow Sand Filtration*. Geneva : World Health Organization, 1974. p. 22.
- Kaeding Performance. Radius rods and Rod ends. [Online] [Cited: 12 9, 2010.] http://www.kaedings.com/index.php?main_page=index&cPath=45.
- Manwell, J F, McGowan, J G and Rogers, A L. 2002. *Wind Energy Explained*. Sussex : J Wiley and sons, 2002.
- Menet, J. L. 2002. *A double-step Savonius rotor for local production of electricity: a design study*. s.l. : Elsevier, 2002. p. 7.
- Muhammad, Nur. 1996. *Optimization of slow sand filtration*. 1996. pp. 1-2.
- United Nations Environment Programme Global Environment Monitoring System. 2007. *Global Drinking Water Quality Index Development and Sensitivity Analysis Report*. Ontario : United Nations Environment Programme Global Environment Monitoring System (GEMS)/Water Programme, 2007. p. 10.
- Ushiyama, I and Nagai, H. 1988. *Optimum design configurations and performances of Savonius rotors*. 1988. pp. 59-75.
- White, Frank M. 2003. *Fluid Mechanics*. 5th edition. New York : McGraw-Hill, 2003. pp. 747-751.
- World Health Organization. 2010. 10 Facts about water scarcity. *World Health Organization*. [Online] May 22, 2010. [Cited: May 22, 2010.] <http://www.who.int/features/factfiles/water/en/>.
- . 2003. *Domestic Water Quantity*. Geneva : World Health Organization, 2003. p. 15.
- . 2009. *World Health Statistics*. s.l. : World Health Organization, 2009. p. 83.

Appendix 12: System Cost

Initial System Cost				
	#	Description	Item Cost	Cost
Turbine and Tower	2	Turbine bearings	\$45.00	\$90.00
	2	4x8 Plywood 1/2in thick	\$15.00	\$30.00
	2	Oil Drums	\$10.00	\$20.00
	2	4x4 20ft long	\$8.00	\$16.00
	1	4x4 8ft long	\$5.00	\$5.00
	100	ft 1/8" Galvanized Cable	\$0.40	\$40.00
	12	Wire loop ends	\$0.50	\$6.00
	12	Wire Crimps	\$0.50	\$6.00
	3	1/4 Turnbuckles 4"long	\$4.00	\$12.00
	1	Hardware	\$13.00	\$13.00
	1	7' steel pipe 1 1/4" ID	\$5.00	\$5.00
	1	Paint	\$10.00	\$10.00
		Subtotal		\$253.00
Pump	2	1" one-way valve (steel)	\$2.50	\$5.00
	2	1" Nipples (steel)	\$2.00	\$4.00
	2	1" Elbows (steel)	\$2.00	\$4.00
	1	Misc steel Parts	\$10.00	\$10.00
	1	Welding Cost	\$20.00	\$20.00
		Subtotal		\$43.00
Slow Sand Filter	40	ft 1" PVC pipe	\$0.50	\$20.00
	3	Oil Drums	\$10.00	\$30.00
	1	Tube of Silicone Sealant	\$5.00	\$5.00
	8	1" PVC Ball valves	\$6.00	\$48.00
	3	1" X style PVC joint	\$1.00	\$3.00
	10	1" PVC elbows	\$0.25	\$2.50
	2	FloatValves	\$15.00	\$30.00
	5	1" PVC stright joints	\$0.25	\$1.25
		Subtotal		\$139.75
Water Storage				
	8	Oil drums	\$10.00	\$80.00
	1	Tube of Silicone Sealant		\$5.00
		Subtotal		\$85.00
			Grand Total	\$520.75
Maintenance cost				
	#	Description	Cost per month	
	1	Lubrication	\$1.00	
	1	Misc Replacement parts	\$10.00	
			Total Monthly Cost	\$11.00